# TECHNICAL NOTE

## D-224

# A TECHNIQUE FOR FIRING DYNAMICALLY SCALED MISSILE MODELS IN WIND TUNNELS AND FOR MEASURING ROCKET-MOTOR SOUND AND PRESSURE FLUCTUATIONS

By William J. Alford, Jr., and Kenneth W. Goodson

Langley Research Center
Langley Field, Va.

NATIONAL AERONAUTICS AND SPACE ADMINISTRATION

WASHINGTON March 1960

NATIONAL AERONAUTICS AND SPACE ADMINISTRATION

TECHNICAL NOTE D-224

# A TECHNIQUE FOR FIRING DYNAMICALLY SCALED MISSILE MODELS IN WIND TUNNELS AND FOR MEASURING ROCKET-MOTOR SOUND AND PRESSURE FLUCTUATIONS

By William J. Alford, Jr., and Kenneth W. Goodson

## SUMMARY

An investigation was made to develop techniques for firing dynamically scaled missile models in wind tunnels and indicated that such techniques are practical. The dynamic-similarity laws were reviewed and found to be applicable to either constant Mach number scaling (equal compressibility characteristics) or constant Froude number scaling (equal acceleration characteristics). Rocket motors were designed that provided reasonable thrust time histories. The photographic instrumentation was adequate for obtaining flight-path records of the missiles under conditions of high longitudinal velocity.

The results indicated that the missile launched from a finite-length launcher attached to an airplane had smaller trajectory deviations than did the missile launched from a zero-length launcher. Increasing the airplane angle of attack caused decreases in the vertical and lateral motions of the missile but caused increases in the rolling motion. Changing the airplane sideslip produced excessively large rolling motions with the largest effects occurring for positive sideslip angle (missile under left wing). Noise measurements of the rocket motor were made and the results showed high overall acoustic levels of approximately 146 decibels which could be detrimental to the surrounding structure if they occurred at the structural natural frequency. The noise frequency spectrum could not be obtained because of the extremely short time histories involved.

## INTRODUCTION

Many airplane and missile manufacturers are involved in the design of air-to-air and other aerial missiles. Although this task is exacting, it becomes even more complex when a missile must be carried, launched, or jettisoned from locations on the airplane where asymmetrical flow conditions exist. These nonuniform flow conditions have been found to induce

large carry loads and to produce deviations in missile flight path that reduce the missile-kill probability and which could, in the worst instance, cause danger to the launching airplane. The possibility of structural damage caused by high-frequency pressure pulsations of a missile rocket motor has also been of concern.

Various phases of the overall missile-airplane combination have been studied by the National Aeronautics and Space Administration and other agencies by means of static wind-tunnel test methods such as determining the aerodynamic characteristics of missiles that operate within the nonuniform flow field of the airplane (see ref. 1) and by studying the flow-field characteristics around various wing-body combinations (refs. 2 to 4). Theoretical studies have also been made of the flow field and its effects on missile characteristics at subsonic and supersonic speeds (refs. 5 and 6).

The purpose of this paper is to describe an additional method for studying the launching of a missile from an airplane; specifically, a method is described for firing dynamically scaled missile models in wind tunnels and for measuring rocket-motor sound and pressure fluctuations. Missile-model trajectory time histories utilizing two different dynamic-scaling criteria are presented and discussed, and a sample record of the rocket-motor transient-noise pressures is included.

## SYMBOLS

The positive directions of angles and distances are shown in figure 1.

| | |
|---|---|
| $a$ | acceleration, $ft/sec^2$ |
| $c$ | speed of sound, ft/sec |
| $F$ | thrust, lb |
| $g$ | gravitational acceleration, 32.2 $ft/sec^2$ |
| $h$ | altitude, ft |
| $I$ | moment of inertia, $slug\text{-}ft^2$ |
| $I_X, I_Y, I_Z$ | moments of inertia about body axes, $slugs\text{-}ft^2$ |
| $l$ | characteristic length, ft |
| $m$ | mass, slugs |

| | |
|---|---|
| M | Mach number, $V/c$ |
| $N_{Fr}$ | Froude number, $\frac{V}{\sqrt{lg}}$ or $\frac{V^2}{lg}$ |
| R | Reynolds number, $\frac{\rho V l}{\mu}$ |
| t | time, sec |
| V | free-stream velocity, ft/sec |
| X,Y,Z | Euler axes |
| x,y,z | distances relative to initial center-of-gravity location on launching airplane along X-, Y-, and Z-axes, respectively, ft |
| $\alpha$ | angle of attack of launching airplane, deg |
| $\alpha'$ | angular acceleration, $deg/sec^2$ |
| $\beta$ | angle of sideslip of launching airplane, deg |
| $\theta$ | angle of pitch, deg |
| $\mu$ | absolute viscosity, $\frac{lb\text{-}sec}{ft^2}$ |
| $\rho$ | air density, $\frac{slugs}{ft^3}$ |
| $\phi$ | angle of roll, deg |
| $\psi$ | angle of yaw, deg |
| $\omega$ | angular velocity, deg/sec |

Subscripts:

| | |
|---|---|
| m | model characteristics |
| fs | full-scale characteristics |

Velocities and accelerations are denoted by single- and double-dotted quantities, respectively.

## MODELS AND APPARATUS

The models used in the investigation consisted of 1/10-scale models of a typical missile and a delta-wing airplane. A drawing showing the general arrangement of the airplane-missile combination is presented in figure 2(a), and a photograph of the models in the Langley 300-MPH 7- by 10-foot tunnel is presented in figure 3. The airplane model was constructed of mahogany and was suspended from the ceiling of the wind tunnel by a swept steel strut. (See fig. 3.) The ogival nose of the missile model was constructed of mahogany and the cylindrical afterbody was made of fiber glass. Earlier versions of the missile model utilized tail fins made of fiber glass, whereas later versions utilized magnesium. The missile wings were also constructed of magnesium. A detail drawing of the missile model is presented in figure 2(b). The missile suspension pylon was constructed of steel with a fiber-glass launching rail. Two versions of the launcher were used: one of zero length and the other of finite length that corresponded to 3 feet, full scale. A detail drawing of the pylon is presented in figure 2(c).



Crystal microphones and a differential pressure gage were imbedded in the airplane-model wing lower surface to obtain the rocket-motor noise and pressure pulsation. The locations of these instruments are shown in figure 2(d). The center line of the missile exit was 1.5 inches below the wing surface.

The rocket motors were designed by the Pilotless Aircraft Research Division of the Langley Research Center. Two rocket designs were employed: type A, used in the constant Mach number simulation, provided an average thrust of 90 pounds for a period of 0.07 second with a jet-exit half-angle of $18.0^{\circ}$; type B, used in the constant Froude number simulation, provided an average thrust of 10.5 pounds for approximately 0.20 second with a jet-exit half-angle of $9.5^{\circ}$. A drawing of the rocket motors is presented in figure 4, and typical static-thrust time histories are presented in figure 5.

The photographic instrumentation is presented in figure 6(a), and a schematic diagram of the complete instrumentation is presented in figure 7.

The programer contained the following:

(1) Controls for regulating the speed of the rotating disks attached to the still cameras which produced multiple-exposure photographs of the missile in flight. Two of these cameras were employed, one of which obtained the side view (fig. 6(a)) and the other, mounted on the top of the wind tunnel, obtained the top view. A typical

multiple-exposure photograph of a missile model in flight is presented in figure 8.

(2) Controls for starting the high-speed movie cameras which were mounted beside the still cameras. For the missile launchings using the constant Mach number simulation the movie-camera speeds were approximately 6,000 frames/sec, and for the constant Froude number simulation the speeds were approximately 1,000 frames/sec.

(3) A turntable starting sequence switch which ignited the illuminating photoflash bulbs.

(4) A sensitive blast galvanometer to check the continuity of the rocket-motor ignition circuit and incorporated two personnel safety features that consisted of a lock switch with removable key (automotive ignition type) and a removable plug switch that inactivated the motor ignition circuit.

An electronic counter was utilized to check the time delays and camera speeds. A timing oscillator was used to provide a known frequency trace for the oscillograph. The outputs of the magnetic pickup installed on the rotating-disk cameras were recorded on the oscillograph along with a record of rocket-motor ignition. A signal of the first motion of the missile, which provided a zero-time datum, was obtained and recorded when the missile suspension lugs, which were also an integral part of the rocket-motor ignition circuit (see detail in fig. 7), moved off of spring contact switches in the supporting pylon.

The noise instrumentation consisted of four crystal microphones and an inductance pressure gage in conjunction with a 14-channel tape recorder. The microphones and the inductance pressure gage were mounted flush with the lower surface (missile side) of the wing. The locations of the microphones and the pressure gage are shown in figure 2(d) and in the photograph in figure 3. A photograph of the tape recorder is shown in figure 6(b). The microphones had a sensitivity of 21 microvolts per dyne per square centimeter, a flat frequency response from 100 to 15,000 cycles/sec (within 3 decibels), and an undisturbed sound-pressure range up to 160 decibels (referred to 0.0002 dyne/cm$^2$). The microphone signals were attenuated a known amount by the cable and fixed capacities to correspond to the dynamic range of the preamplifiers. The attenuation of a given microphone signal could be varied in 3-decibel increments and fed in parallel to several recorder channels to insure a good recording. The signals were directly recorded at a tape speed of 30 in./sec. The frequency range was 100 to 50,000 cycles/sec.

The inductance pressure gage had a range of 1/2 lb/sq in. and when used with a 20-kilocycle carrier amplifier has a flat frequency

response from 0 to above 1,000 cycles/sec. The pressure gage is sensitive to a change in pressure level as well as to fluctuating pressures. The inductance gage was used to measure the low-frequency pressure fluctuations. The frequency-modulation signal (FM) is recorded at a center frequency of 27 kilocycles and at 30 in./sec which gives a frequency range of 0 to 5,000 cycles/sec. The zero-time pulse (fig. 7) of the model leaving the launcher was also recorded on the tape recorder.

In order to obtain a time history of the noise pressure and timing signals, the tape is played back at 15 in./sec and all channels are recorded by using frequency modulation at 27 kilocycles and 30 in./sec. The new record then is played back at $3\frac{3}{4}$ in./sec, and the signal is recorded on an oscillograph with standard galvanometers. The previous operations on the signals are necessary so that no frequencies of importance are lost and the signal-to-noise ratio is maintained while the time scale is expanded 16 times.



## TESTS

The tests were conducted in the Langley 300-MPH 7- by 10-foot tunnel. Four missiles were launched by using the constant Mach number simulation with a free-stream velocity of 300 ft/sec which corresponded to a Mach number of 0.27 and a Reynolds number of $2.2 \times 10^6$ based on missile-model length. Eight missile models were launched by using the constant Froude number simulation with a free-stream velocity of 275 ft/sec (which corresponded to a full-scale free-stream velocity of 866 ft/sec) and a Reynolds number of $2.1 \times 10^6$.

The tests made by using constant Mach number similarity were useful in determining the suitability of the photographic instrumentation for obtaining trajectory records under conditions of high longitudinal acceleration (up to approximately 530g model scale). Because of the low Mach number (M = 0.27) of the tests the trajectory results are of little quantitative value since the angle of attack employed did not correspond to that required for flight at the assumed altitude. All of these firings used a finite-length launcher. The effects of changing launching-airplane angle of attack and sideslip as well as the effect of launching-rail length were investigated by using the constant Froude number criterion.

## DYNAMIC-SIMILARITY SCALING PARAMETERS

Unpublished studies made at the Langley Research Center have indicated that the problems of dynamic similitude in model testing are multifold and generally controversial with the result that a considerable volume of literature has accrued. (See, for instance, refs. 7 to 11.) The problems might be considered as being of one order greater than those of fixed-model testing where only the path of motion of air about the model need be similar to those about the full-scale body. In dynamic testing the additional requirement is that the path of motion of the model be similar to the path of the full-scale body. In simplest form (without regard to heat conduction, transfer, etc.) the Reynolds number R and Mach number M of the air flow about the model and the full-scale body must be the same in addition to the model having geometric similarity to the full-scale body including surface roughness and flexibility. In free-model testing the kinematics of the body are introduced and it is necessary that the mass and mass distribution of the model be scaled properly. The model must also respond correctly to gravitational forces, as required by the Froude number $N_{Fr}$. A general law of dynamic similarity would, therefore, require that each of the similarity numbers or separate laws be the same for model and full-scale bodies. Consideration of the three scaling parameters ($R$, $M$, and $N_{Fr}$) indicates that a general law is impractical, if not impossible.

The general practice is, therefore, to assume that differences in model and full-scale Reynolds numbers have a negligible effect and, hence, the aerodynamic characteristics are identical. For lightly loaded objects this assumption should be adequately considered in interpretation of the results of dynamic-model tests. Even with the simplifying assumption of equal Reynolds numbers an incompatibility arises in attempting to satisfy both the Mach number and Froude number in that the Mach number requires that velocities of the model and full-scale body be approximately the same with the result that all model linear accelerations should be increased by the scale factor $l_{fs}/l_m$ (ref. 9). In contrast to Mach number, the Froude number requires that all linear accelerations of the model and full-scale body must be equal, with the result that the velocity of the model free stream must be reduced by the square root of the scale factor (ref. 8). With constant Mach number simulation the vertical acceleration of the model is too small for dynamic similarity inasmuch as the acceleration due to gravity cannot be altered. With constant Froude number simulation compressibility effects cannot be duplicated because of unequal Mach numbers. Because of the aforementioned incompatabilities, both methods were employed in the present investigation.

The complete derivation of the scaling parameters is included in several papers; however, the methods of references 8 and 9 were used in

the present investigation. For completeness, the pertinent factors are listed as follows:

| Item | Constant Mach number | Constant Froude number |
|---|---|---|
| Helix angle . . . . . | $\frac{\omega_{fs} l_{fs}}{V_{fs}} = \frac{\omega_m l_m}{V_m}$ | $\frac{\omega_{fs} l_{fs}}{V_{fs}} = \frac{\omega_m l_m}{V_m}$ |
| Angular velocity . . . . . | $\frac{\omega_{fs}}{\omega_m} = \frac{V_{fs}}{V_m} \frac{l_m}{l_{fs}}$ | $\frac{\omega_{fs}}{\omega_m} = \frac{V_{fs}}{V_m} \frac{l_m}{l_{fs}} = \sqrt{\frac{l_m}{l_{fs}}}$ |
| Linear velocity . . . . . | $\frac{V_{fs}}{V_m} = \frac{c_{fs}}{c_m}$ | $\frac{V_{fs}}{V_m} = \sqrt{\frac{l_{fs}}{l_m}}$ |
| Linear acceleration . . . . | $\frac{a_{fs}}{a_m} = \left(\frac{c_{fs}}{c_m}\right)^2 \frac{l_m}{l_{fs}}$ | $\frac{a_{fs}}{a_m} = 1$ |
| Angular acceleration . . . | $\frac{\alpha'_{fs}}{\alpha'_m} = \frac{a_{fs}}{a_m} \frac{l_m}{l_{fs}}$ | $\frac{\alpha'_{fs}}{\alpha'_m} = \frac{l_m}{l_{fs}}$ |
| Mass . . . . . | $\frac{m_{fs}}{m_m} = \left(\frac{l_{fs}}{l_m}\right)^3 \frac{\rho_{fs}}{\rho_m}$ | $\frac{m_{fs}}{m_m} = \left(\frac{l_{fs}}{l_m}\right)^3 \frac{\rho_{fs}}{\rho_m}$* |
| Inertia . . . . . | $\frac{I_{fs}}{I_m} = \left(\frac{l_{fs}}{l_m}\right)^5 \frac{\rho_{fs}}{\rho_m}$ | $\frac{I_{fs}}{I_m} = \left(\frac{l_{fs}}{l_m}\right)^5 \frac{\rho_{fs}}{\rho_m}$* |
| Time . . . . . | $\frac{t_{fs}}{t_m} = \frac{c_m}{c_{fs}} \frac{l_{fs}}{l_m}$ | $\frac{t_{fs}}{t_m} = \sqrt{\frac{l_{fs}}{l_m}}$ |

*The density ratio $\rho_{fs}/\rho_m$ was considered as unity in reference 8.

It should be noted that the model mass and inertia scaling parameters are the same for both scaling methods.

The mass and inertia characteristics of the full-scale missile considered in the present investigation were as follows:
$m = 10.15$ slugs; $I_Y = I_Z = 96.5$ slug-ft$^2$; $I_X = 0.85$ slug-ft$^2$;

center-of-gravity location = 0.555$l$. The mass of the missile model was determined by weighing the model on sensitive laboratory scales, and the center-of-gravity location was determined by balancing the model on a knife edge. The mass moments of inertia about the model principal axes (which due to symmetry corresponded to the body axes) were determined from the calibrated periods of torsion pendulums.

For all models used in the investigation, which were ballasted to simulate launching at an altitude of 10,000 feet, the maximum error is given as follows: In mass it was less than 1/2 percent, in the center-of-gravity location it was less than 1 percent, in $I_Y = I_Z$ it was less than 1/2 percent, and in $I_X$ it was less than 8 percent. The additional mass corrections due to ambient air conditions were calculated by use of the method of reference 12 and were found to be negligible.

## RESULTS AND DISCUSSION

The missile-trajectory displacements were obtained from the photographic records and were correlated with time. These results were graphically differentiated to obtain velocities and accelerations. The results are presented as full-scale time histories in figures 9 to 16.

### Constant Mach Number Simulation

The photographic instrumentation proved to be adequate in that records were obtained on three out of four missiles that were fired. Motion-picture speeds on the order of 6,000 frames/sec were utilized.

A comparison of the rounds using the constant Mach number simulation technique in figures 9, 10, and 11 indicates, in general, that the effect of increasing the free-stream velocity from 0 (fig. 9) to 300 ft/sec (figs. 10 and 11) had only a small effect on the missile trajectories. The notable exception was round 3 (fig. 10) which exhibited a considerably higher longitudinal acceleration than did rounds 2 and 4. The large difference in longitudinal accelerations of the various missiles indicates large variations in rocket-motor thrust which might be attributed to changes in propellant characteristics between the various rounds. The tail fins of these models were constructed of fiber glass and incurred a noticeable degree of warpage. This warpage, rather than the aerodynamic inputs from the launching-airplane flow field, is felt to be the cause of the small variations that occurred in motions along the Z- and Y-axes inasmuch as the forward accelerations of the model were so high. In order to eliminate the tail-fin warpage, the remaining missiles had tail fins that were constructed of magnesium.

## Constant Froude Number Simulation

In general, the time histories of the missile trajectory exhibited larger vertical and lateral accelerations with the zero-length launcher (fig. 13) than with the finite-length launcher (fig. 12). For instance, the peak vertical acceleration for the zero-length launcher was approximately 10g as compared with approximately 7.5g for the finite-length launcher.

Increasing the airplane angle of attack for the rounds using the constant Froude number technique (compare figs. 13 and 14) caused decreases in the vertical and lateral motions but caused increases in the rolling motion. This latter result is as would be expected because of the increase in both the strength and gradients of the airplane-induced flow field. The reduction in the vertical and lateral motions is not understood inasmuch as previous investigations (refs. 1 to 3) indicate that increases would be expected.

Changing the airplane sideslip angle produced large changes in the missile-trajectory characteristics (figs. 13, 15, and 16) with the largest changes occurring for the positive sideslip angle. Inasmuch as the missile was under the left wing, the lateral-flow velocities (which are in an outboard direction for the zero-sideslip condition) are increased and the missile lateral motions are accentuated. Excessively large rolling accelerations are incurred for the positive sideslip angle (fig. 15(b)). For the negative sideslip angle (fig. 16(b)) the lateral parameters are generally of the opposite sign and are considerably lower than those for the positive sideslip angle although the rolling rates are still large.

## Rocket-Motor Noise

The noise records obtained with the tape recorder showed that the instrumentation was adequate for obtaining time-history traces of the overall noise level. Unfortunately, the time histories were of such short duration (about 0.06 second) that a frequency-spectrum analysis could not be made. A typical noise time history of the missile rocket motor traversing the lower surface of the wing is shown in figure 17. The trace of the trailing-edge microphone shows that the noise began as the missile left the launcher (zero-time pulse) or slightly before as would be expected since this microphone was located in the jet (noise) cone. Signals from the other microphones (leading-edge and midchord locations) were picked up as the missile traversed the wing lower surface.

The peak noise level at each microphone location was obtained from the peak amplitude of each trace. These peak noise levels varied from

144.1 to 149.2 decibels (fig. 17) which corresponds to a fluctuating noise pressure of about 5.2 lb/sq ft to 11.8 lb/sq ft, respectively. Noise levels of this magnitude or higher can cause structural failure if the frequency range occurs at the natural frequency of the structure (ref. 13). References 14, 15, and 16 indicate that overall noise levels measured on small models correlate well with measurements on larger size motors for a given distance-to-diameter ratio, if the jet-velocity and jet-noise angles are the same; thus, it is indicated that the present results can be used in estimating noise loads on a full-scale airplane. The exit velocity for the present motor was 6,500 ft/sec and the exit angle was 19°. It should be pointed out, however, that the noise level of jets occurs at frequencies which vary inversely with size or scale (refs. 14 and 15); therefore, when using model results to estimate full-scale noise loads, the effects of frequency on the full-scale structure should be considered.

The inductance pressure gage (midchord pressure gage) mounted in the same relative streamwise location as the midchord microphone shows that the noise for both occurred at the same relative location on the time-history trace. (See fig. 17.) The pressure gage also shows a displacement in the trace which is attributed to the higher static-pressure level in the supersonic jet of the rocket engine.

## CONCLUDING REMARKS

An investigation which was made to develop techniques for firing dynamically scaled missile models in wind tunnels indicated that such techniques are practical. The dynamic-similarity laws were reviewed and found to be applicable to either constant Mach number scaling (equal compressibility characteristics) or constant Froude number scaling (equal acceleration characteristics). Rocket motors were designed that provided reasonable scaled thrust time histories. The photographic instrumentation proved adequate for obtaining flight-path records for the missiles under conditions of high longitudinal velocity.

The results indicated that the 1/10-scale model of a typical missile launched from a finite-length launcher attached to a 1/10-scale model of a delta-wing airplane had smaller trajectory deviations than did the missile launched from a zero-length launcher. Increasing the airplane angle of attack caused decreases in the vertical and lateral motions of the missile but caused increases in the rolling motion. Changing the airplane sideslip angle produced excessively large rolling motions with the largest effects occurring for the positive sideslip angle (missile under left wing).

Noise measurements were made and the results showed high overall acoustic levels (approximately 146 decibels) capable of exciting airplane

structures as rocket missiles are launched. A frequency spectrum of the noise could not be obtained from the model results because of the extremely short time histories involved.

Langley Research Center,
National Aeronautics and Space Administration,
Langley Field, Va., November 10, 1959.

## REFERENCES


1. Alford, William J., Jr., and King, Thomas J., Jr.: Experimental Static Aerodynamic Forces and Moments at High Subsonic Speeds on a Missile Model During Simulated Launching From Unswept-, Sweptback-, and Modified-Delta-Wing—Fuselage Combinations at Zero Sideslip. NACA RM L57B04, 1957.

2. Alford, William J., Jr., and King, Thomas J., Jr.: Experimental Investigation of Flow Fields at Zero Sideslip Near Swept- and Unswept-Wing—Fuselage Combinations at Low Speed. NACA RM L56J19, 1957.

3. Alford, William J., Jr., and King, Thomas J., Jr.: Experimental Investigation of Effects of Moderate Sideslip on the Flow Fields Near a 45° Swept-Wing—Fuselage Combination at Low Speed. NACA RM L57E10, 1957.

4. Alford, William J., Jr.: Theoretical and Experimental Investigation of the Subsonic-Flow Fields Beneath Swept and Unswept Wings With Tables of Vortex-Induced Velocities. NACA Rep. 1327, 1957. (Supersedes NACA TN 3738.)

5. Alford, William J., Jr.: Effects of Wing-Fuselage Flow Fields on Missile Loads at Subsonic Speeds. NACA RM L55E10a, 1955.

6. Elliott, Jarrell R., Bobbitt, Percy J., and Goodwin, Julia M.: Theoretical and Experimental Aircraft Induced Forces and Moments on a Cruciform Missile at a Mach Number of Approximately 1.60 and Their Effects on the Missile Trajectory. NASA MEMO 5-17-59L, 1959.

7. Murphy, Glenn: Similitude in Engineering. The Ronald Press Co., 1950.

8. Scherberg, Max, and Rhode, R. V.: Mass Distribution and Performance of Free Flight Models. NACA TN 268, 1927.

9. Neihouse, Anshal I., and Pepoon, Philip W.: Dynamic Similitude Between a Model and a Full-Scale Body for Model Investigation at Full-Scale Mach Number. NACA TN 2062, 1950.

10. Sandahl, Carl A., and Faget, Maxime A.: Similitude Relations for Free-Model Wind-Tunnel Studies of Store-Dropping Problems. NACA TN 3907, 1957.

11. Deitchman, Seymour J.: A Method for Examination of Store Separation From Aircraft Through Dynamic Model Testing at Full-Scale Mach Number. Jour. Aero. Sci., vol. 24, no. 4, Apr. 1957, pp. 275-280.

12. Malvestuto, Frank S., Jr., and Gale, Lawrence J.: Formulas for Additional Mass Corrections to the Moments of Inertia of Airplanes. NACA TN 1187, 1947.

13. Hess, Robert W., Lassiter, Leslie W., and Hubbard, Harvey H.: A Study of the Response of Panels to Random Acoustic Excitation. NACA RM L55E13c, 1955.

14. Mayes, William H.: Some Near- and Far-Field Noise Measurements for Rocket Engines Operating at Different Nozzle Pressure Ratios. Jour. Acous. Soc. of America, vol. 31, no. 7, July 1959, pp. 1013-1015.

15. Fowell, L. R., and Korbacher, G. K.: A Review of Aerodynamic Noise. UTIA Rev., no. 8, Inst. Aerophysics, Univ. of Toronto, July 1955.

16. Mayes, William H., Lanford, Wade E., and Hubbard, Harvey H.: Near-Field and Far-Field Noise Surveys of Solid-Fuel Rocket Engines for a Range of Nozzle Exit Pressures. NASA TN D-21, 1959.

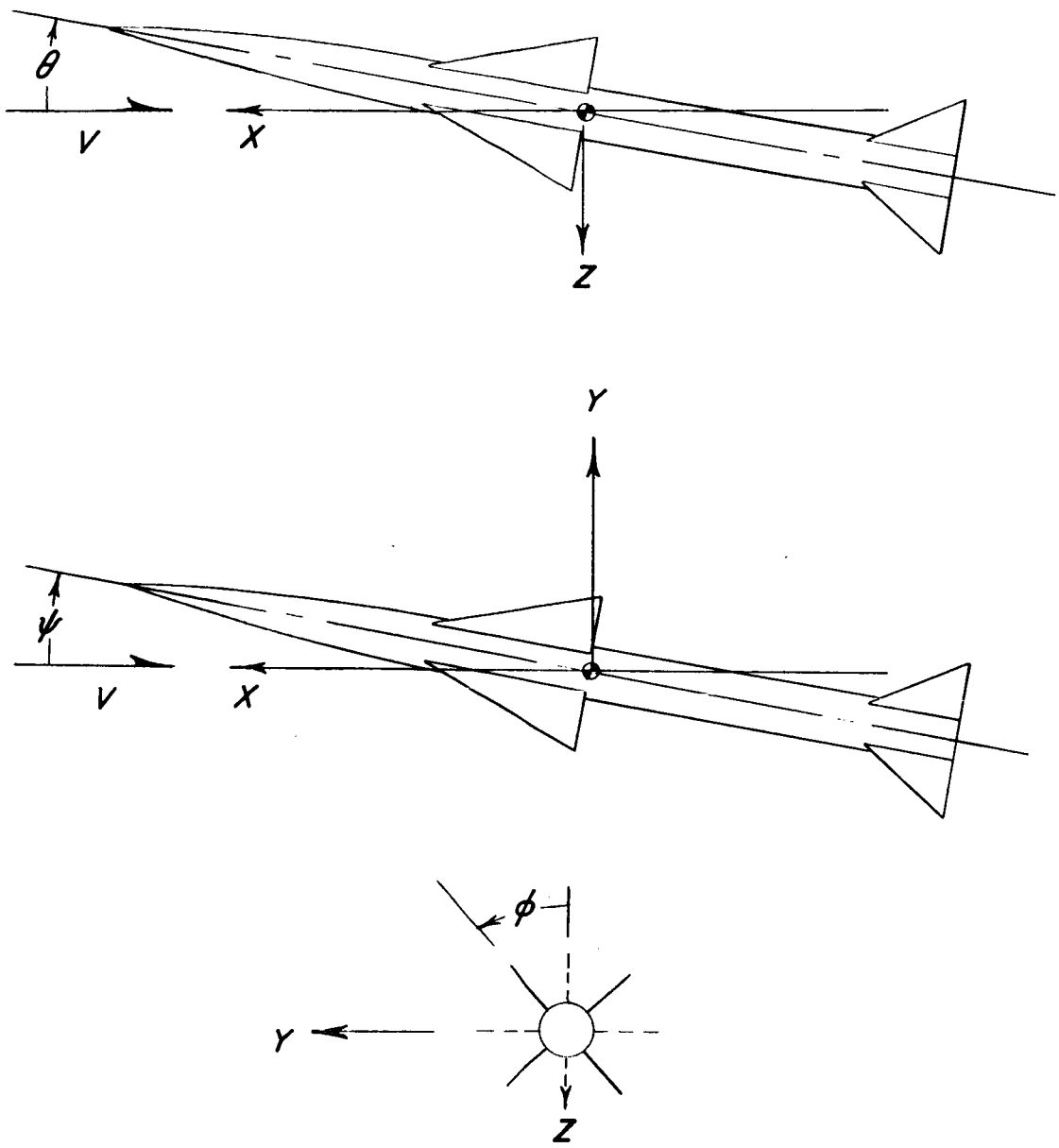


Figure 1.- System of axes used in the investigation. Positive directions of angles and distances are shown by arrows.

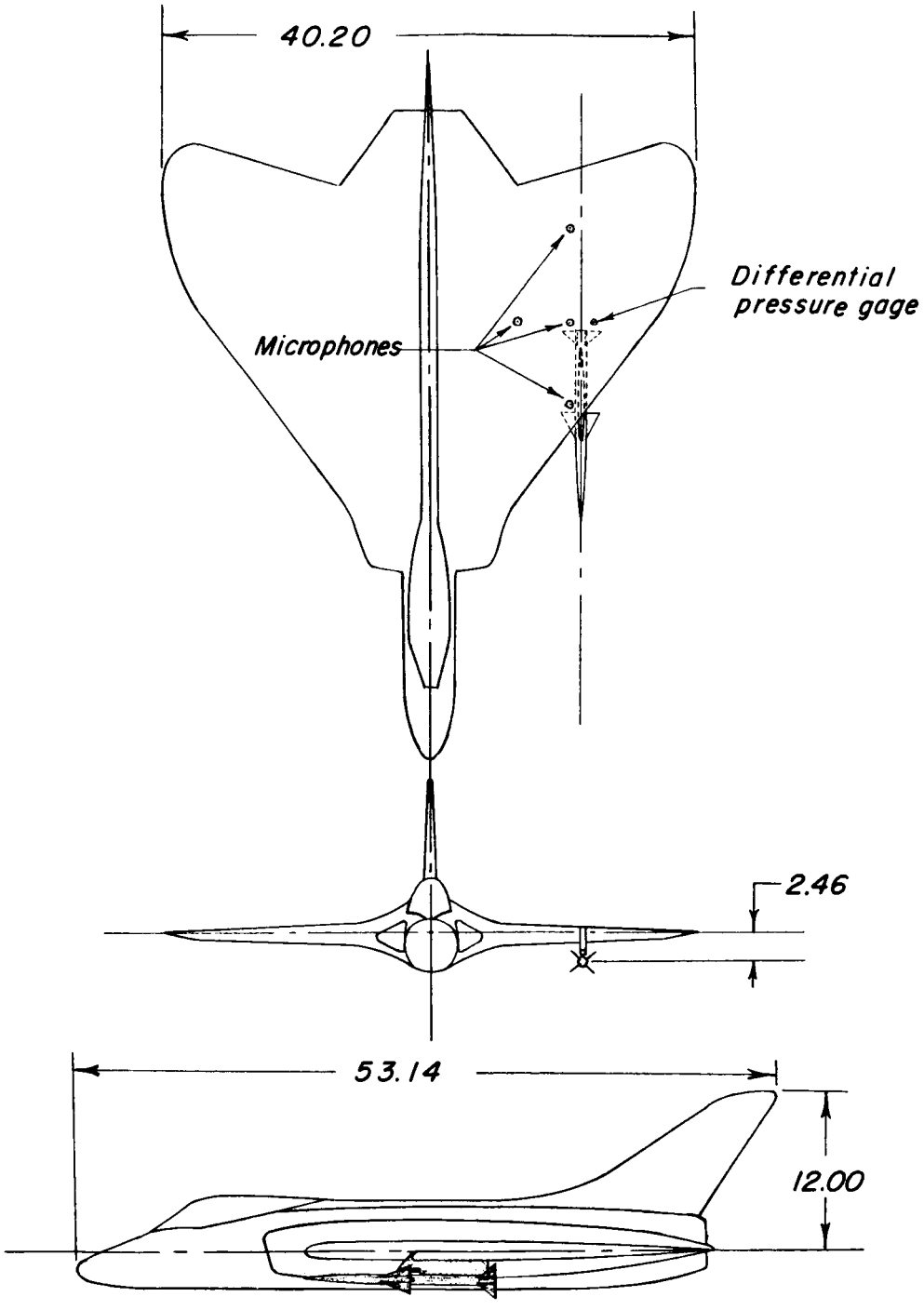


(a) General arrangement of airplane and missile models.

Figure 2.- Drawings of models. All dimensions are in inches.

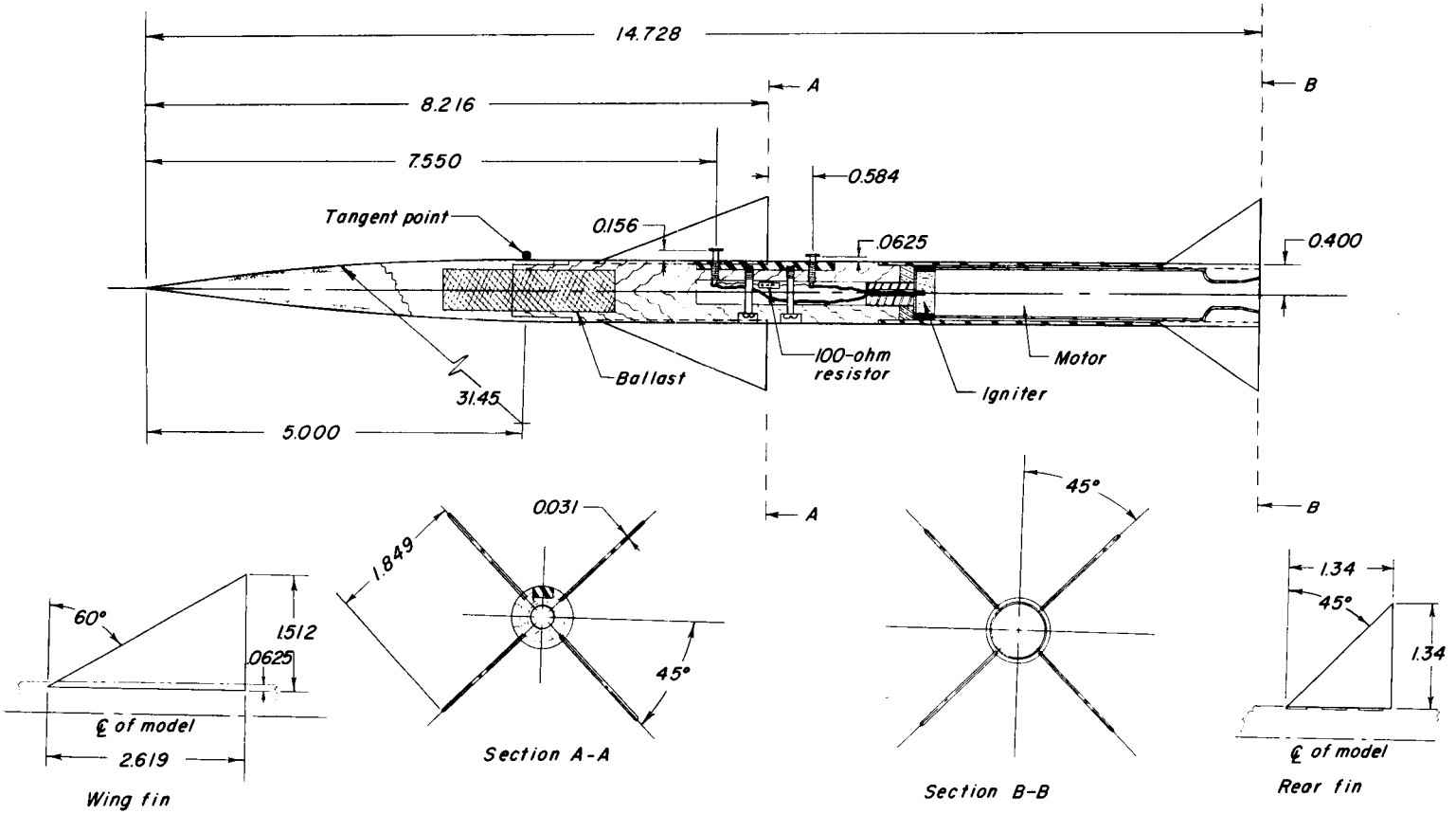


(b) Detail drawing of missile model.

Figure 2.- Continued.

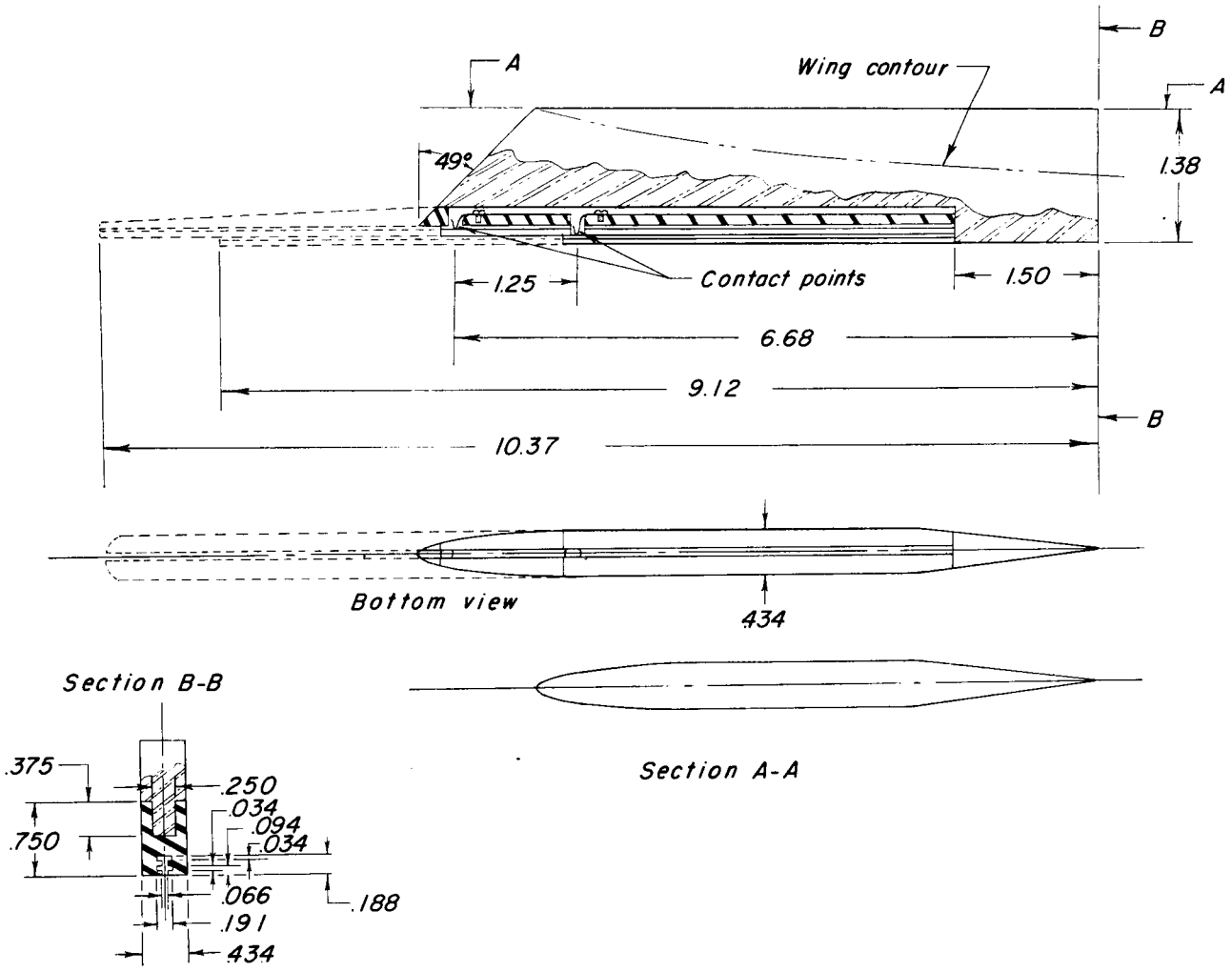


(c) Detail drawing of pylon.

Figure 2.- Continued.

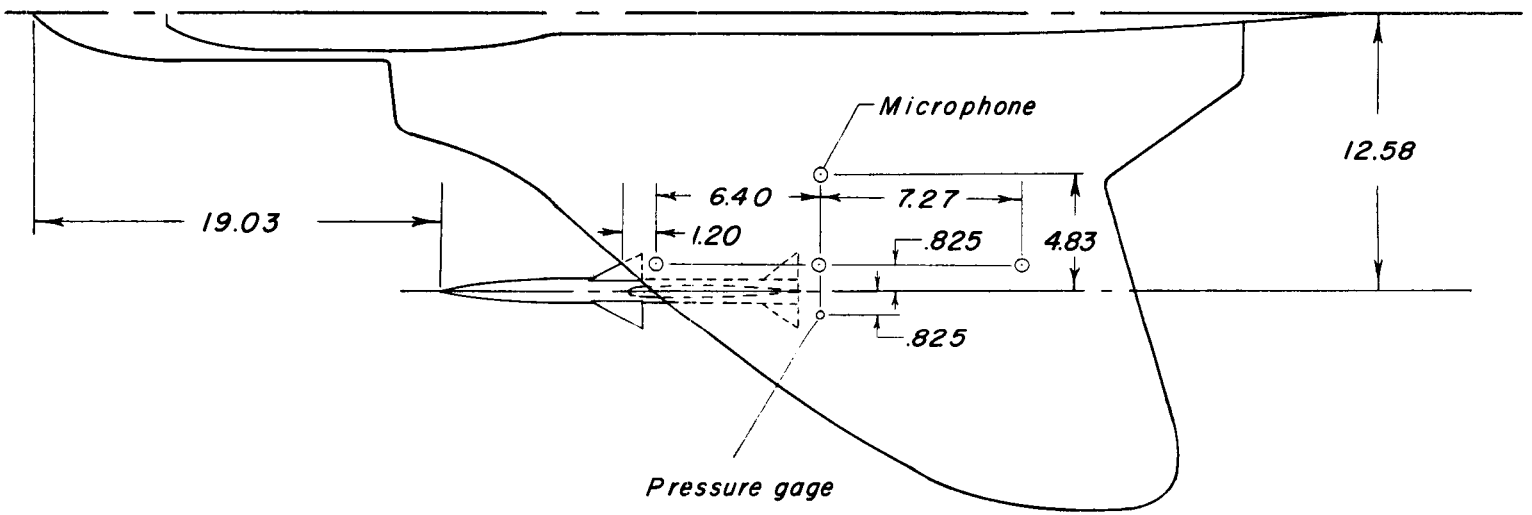


(d) Locations of crystal microphones and pressure gage.

Figure 2.- Concluded.

Figure 3.- Photograph of models in wind tunnel. L-94295

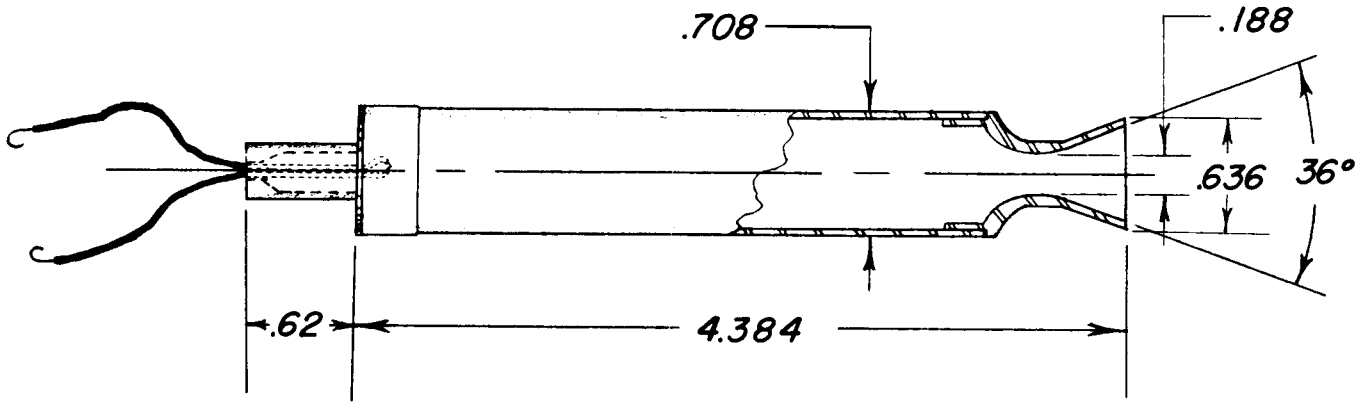


Type A

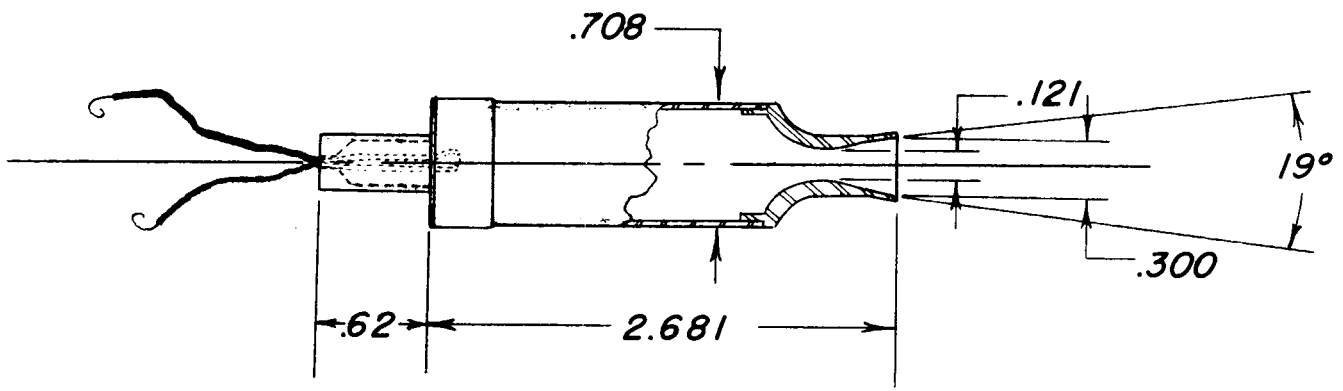


Type B

Figure 4.- Drawing of rocket motors.

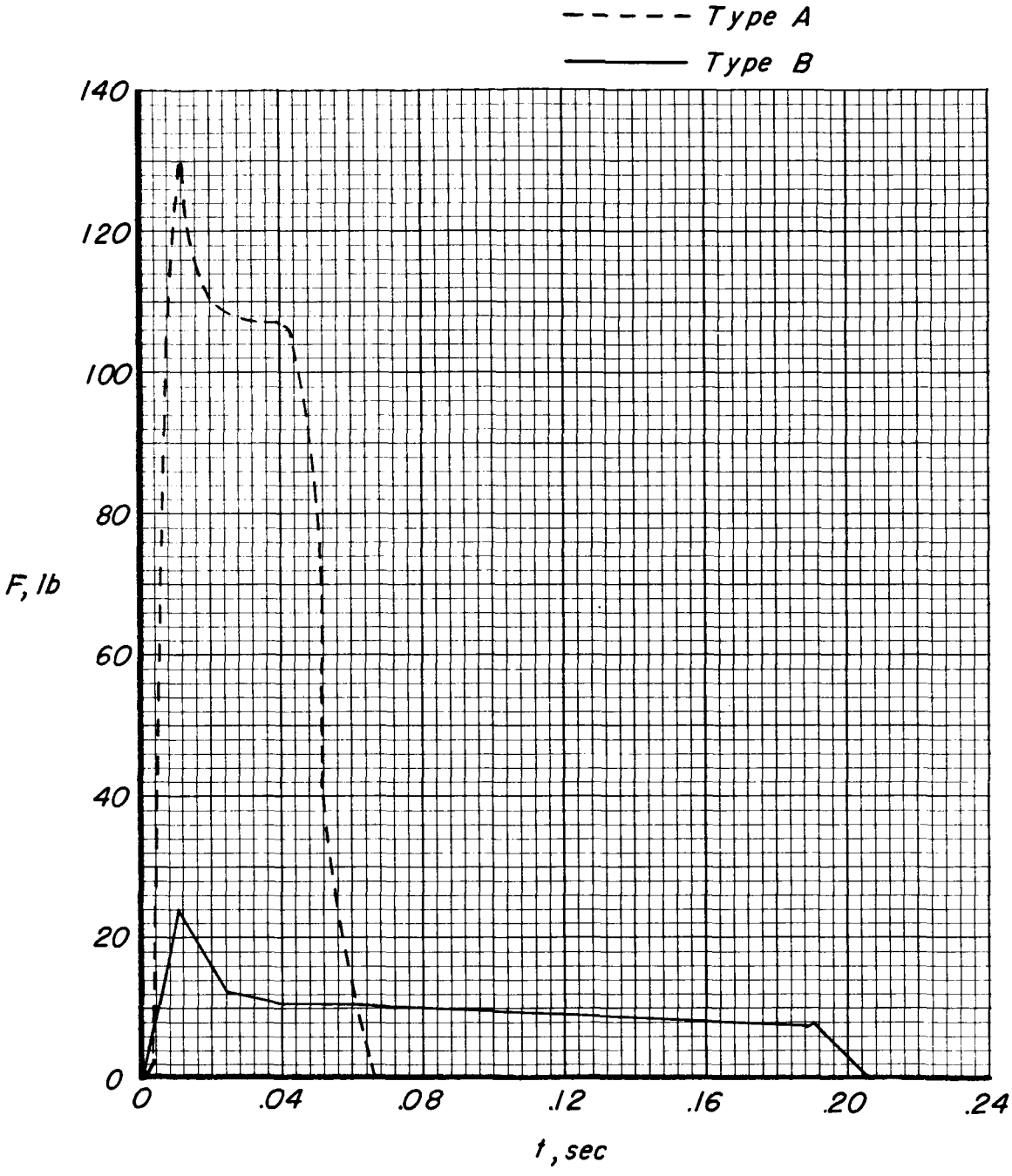


Figure 5.- Typical static-thrust time histories of rocket motors.

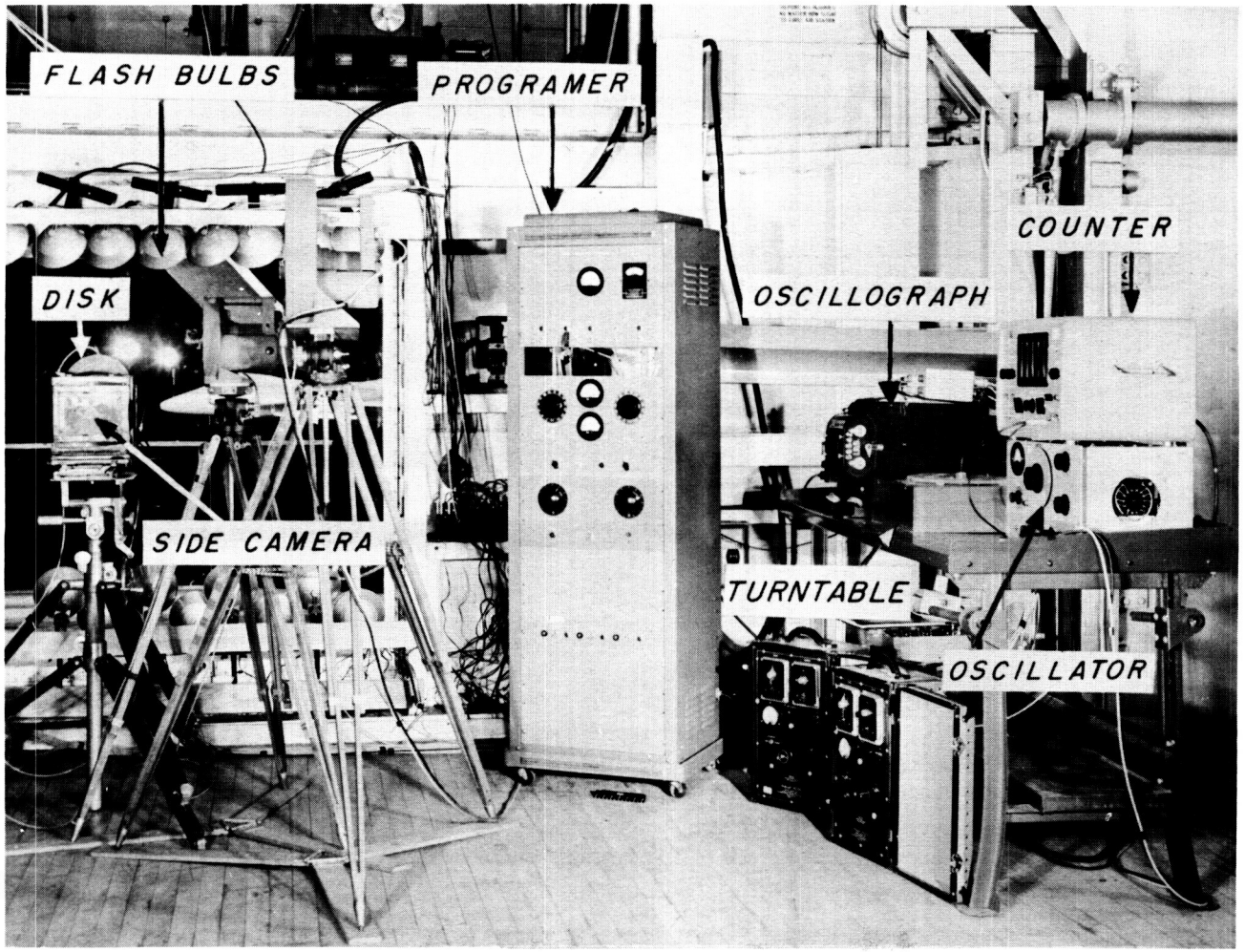


(a) Photographic instrumentation. L-93471.1

Figure 6.- Photographs of instrumentation.

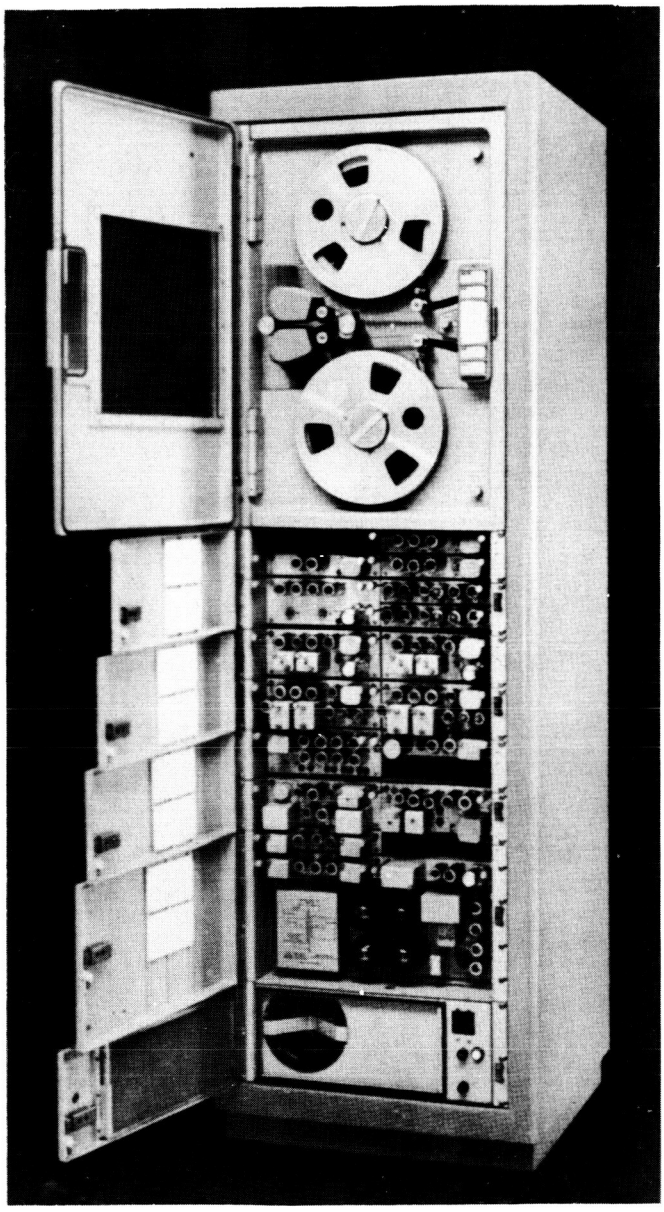

(b) 14-channel magnetic tape recorder. L-59-6491

Figure 6.- Concluded.

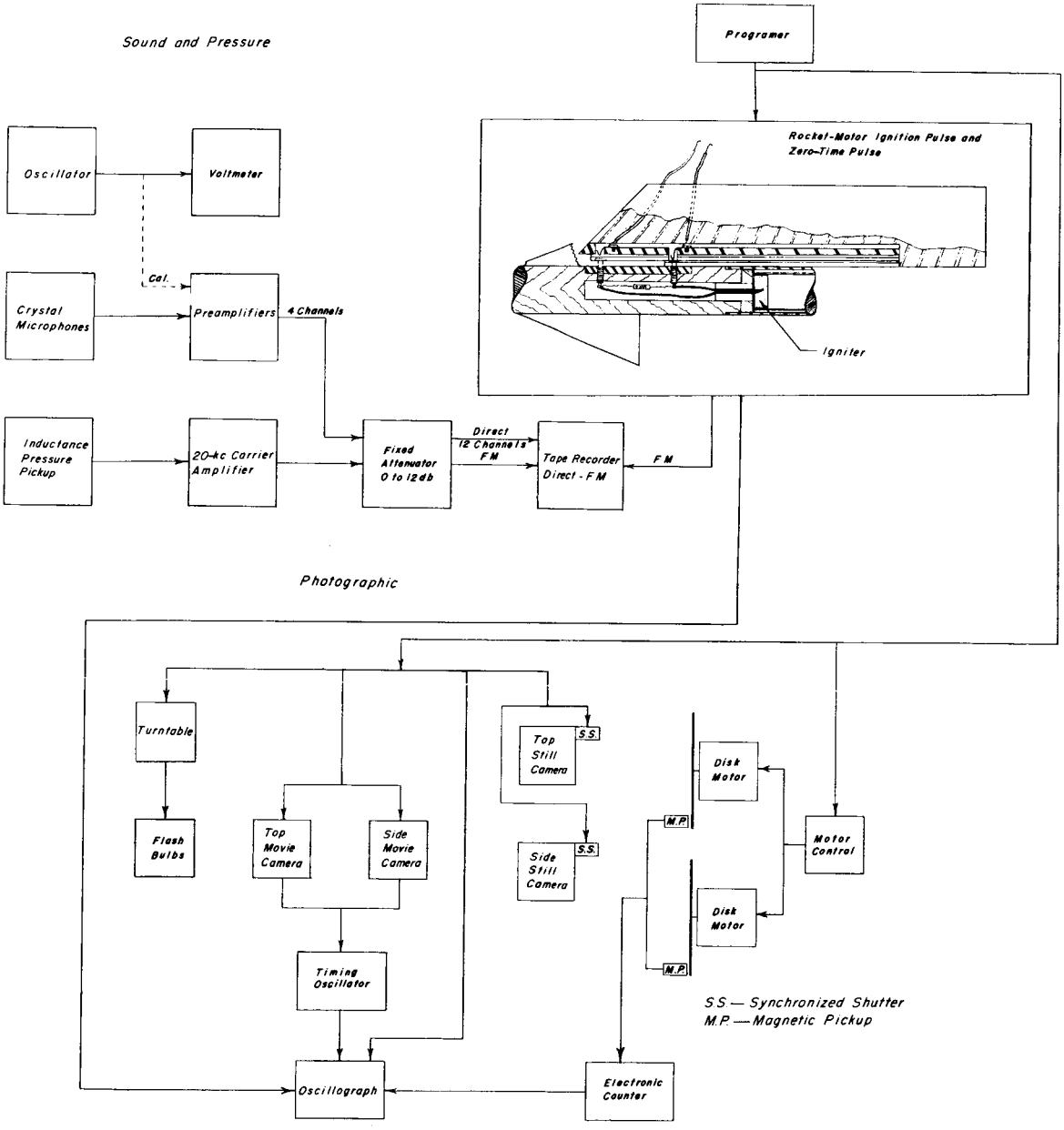


Figure 7.- Schematic diagram of complete instrumentation.

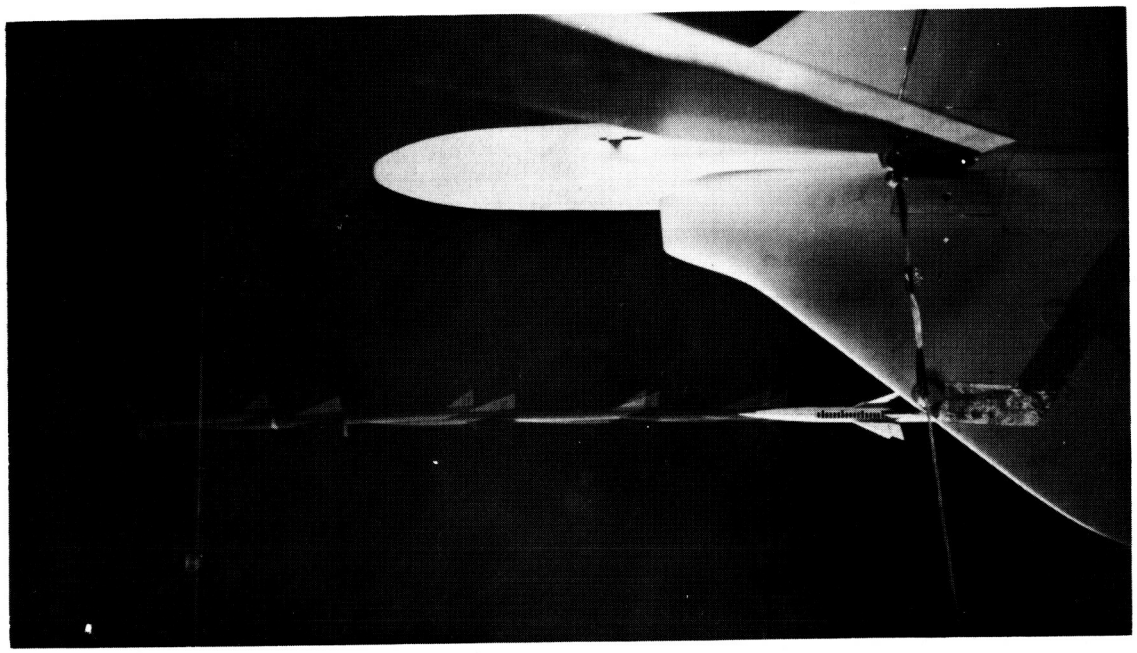

(a) Top view.

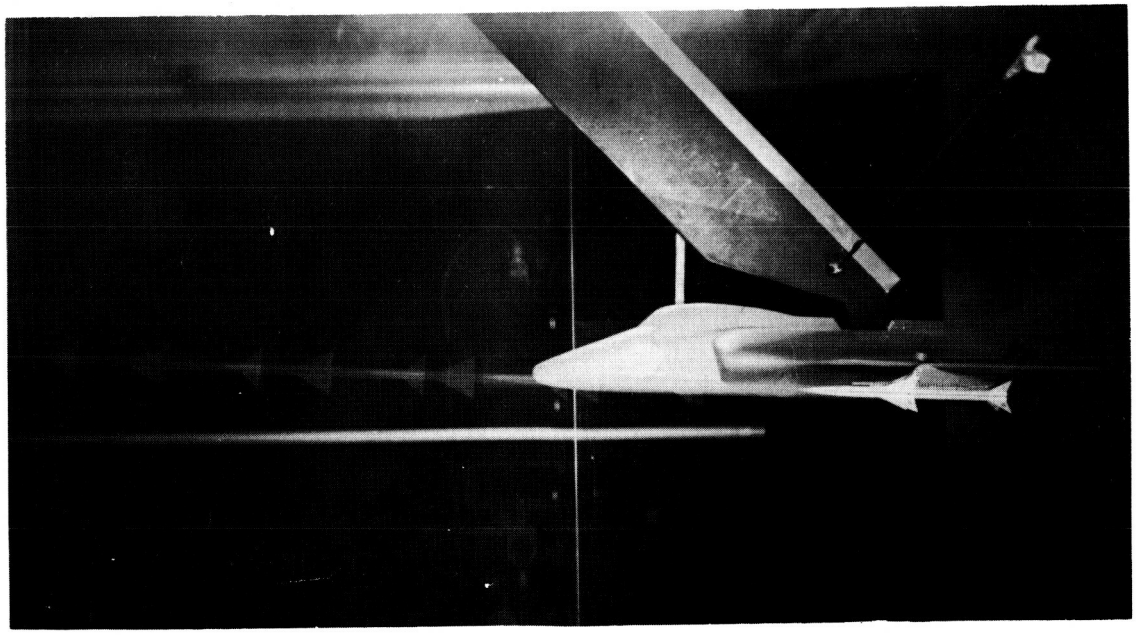

(b) Side view. L-59-6492

Figure 8.- Photograph of typical missile-model launching.

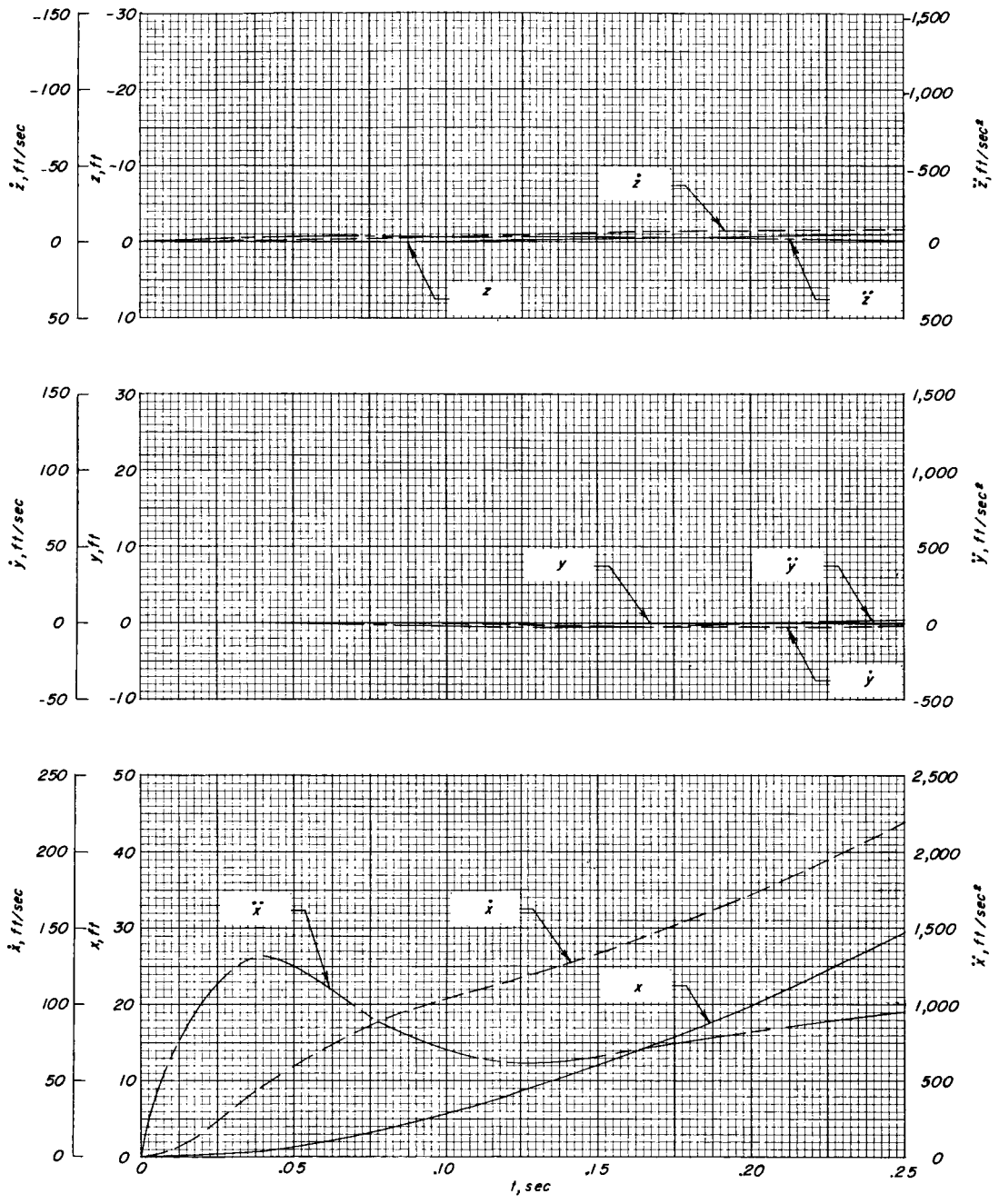


(a) Linear characteristics.

Figure 9.- Trajectory of round 2. Constant Mach number simulation; wind off; $\theta = 2.5^{\circ}$; $\psi = 0^{\circ}$; finite-length launcher.

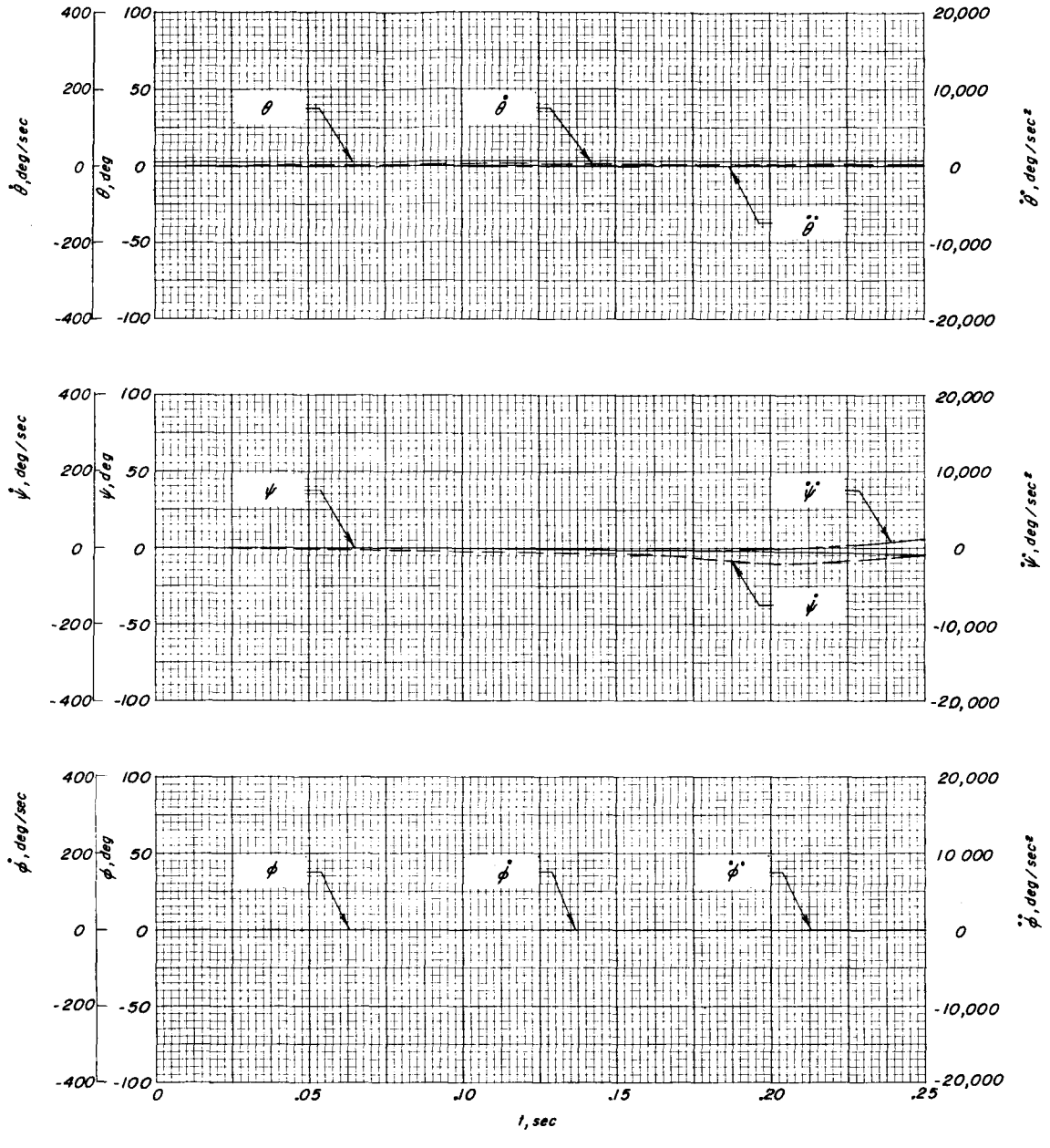


(b) Rotational characteristics.

Figure 9.- Concluded.

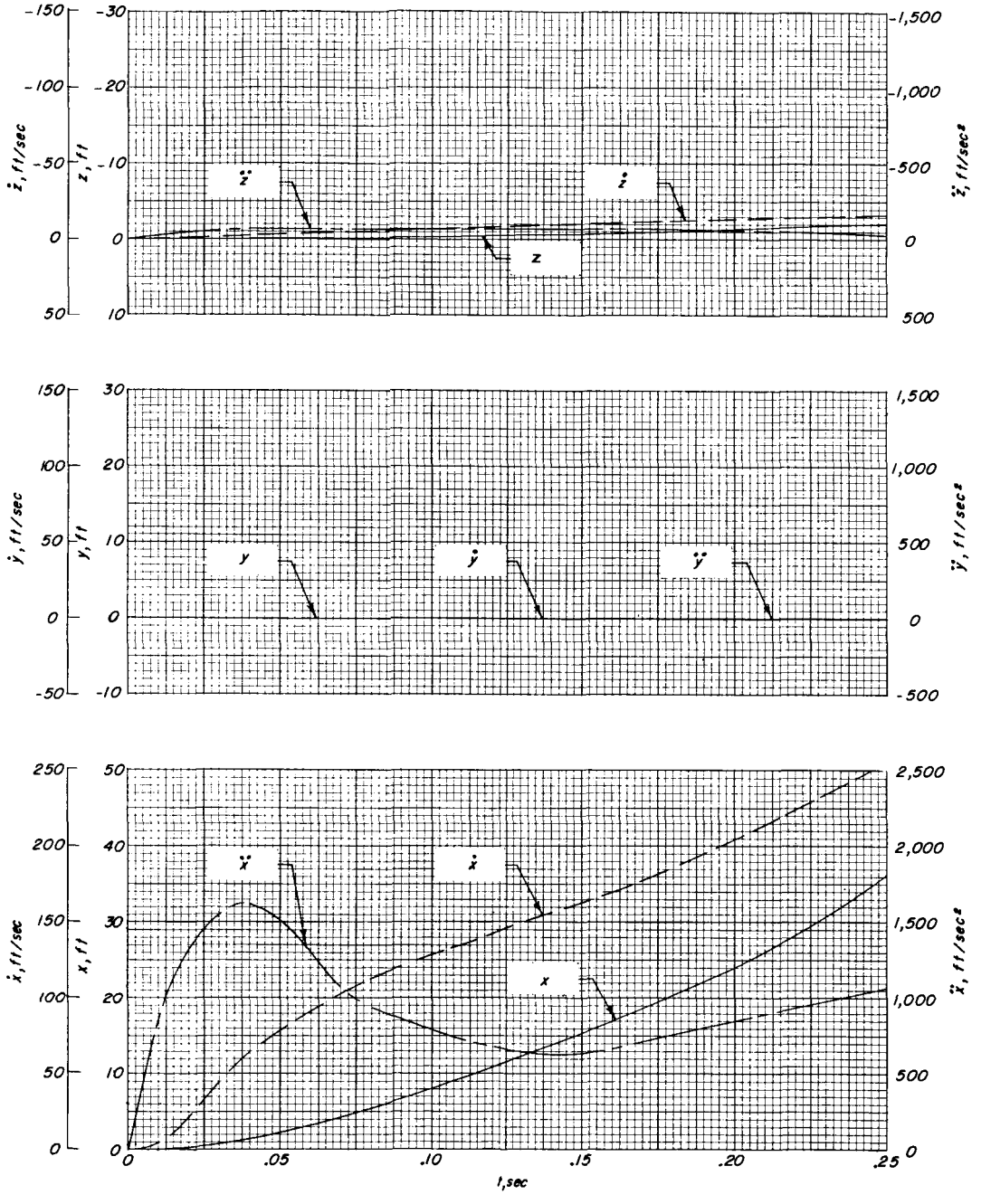


(a) Linear characteristics.

Figure 10.- Trajectory of round 3. Constant Mach number simulation; $h \approx 10{,}000$ feet; $M \approx 0.27$; $\alpha = 2.5^{\circ}$; $\beta = 0^{\circ}$; finite-length launcher.

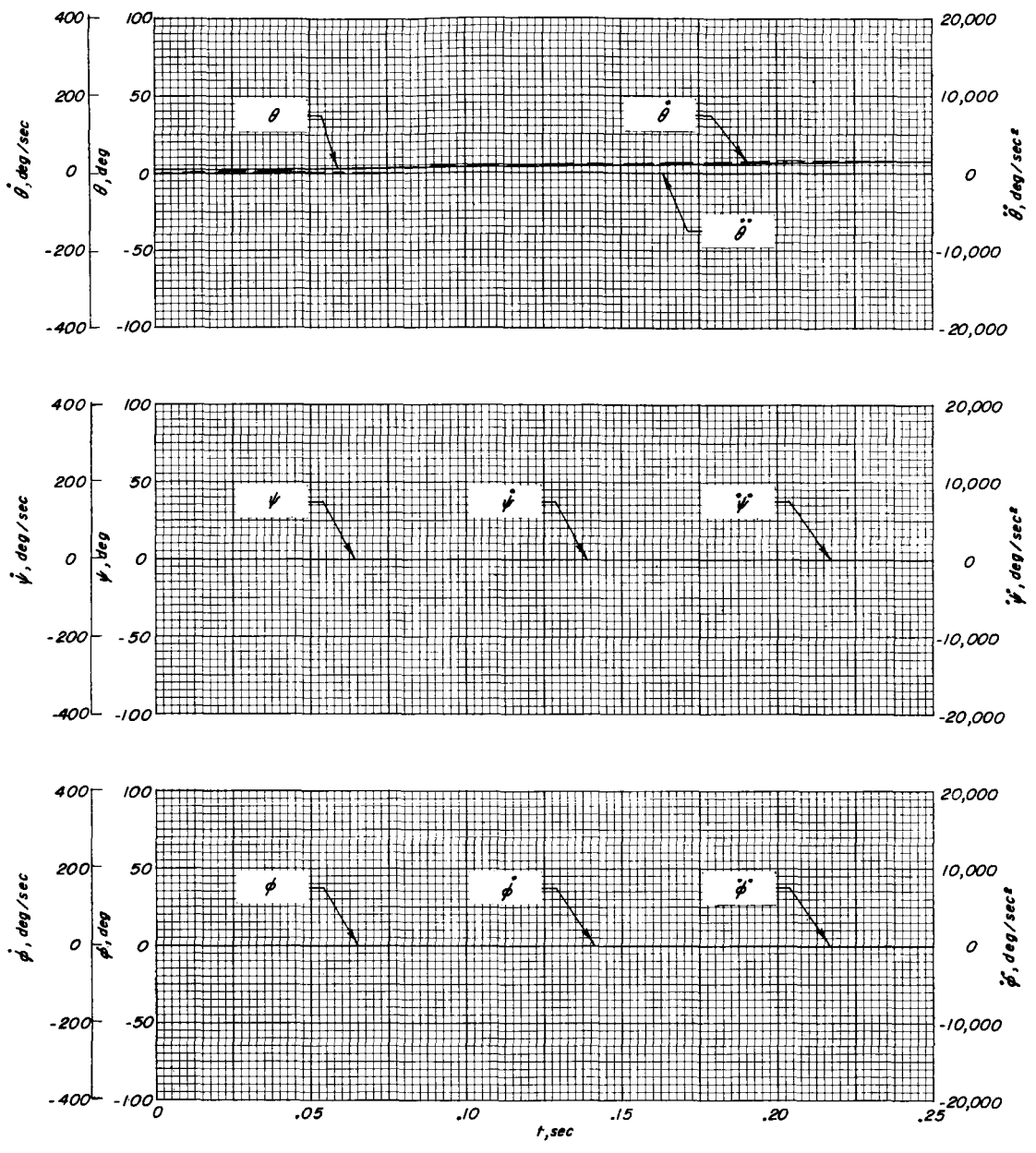


(b) Rotational characteristics.

Figure 10.- Concluded.

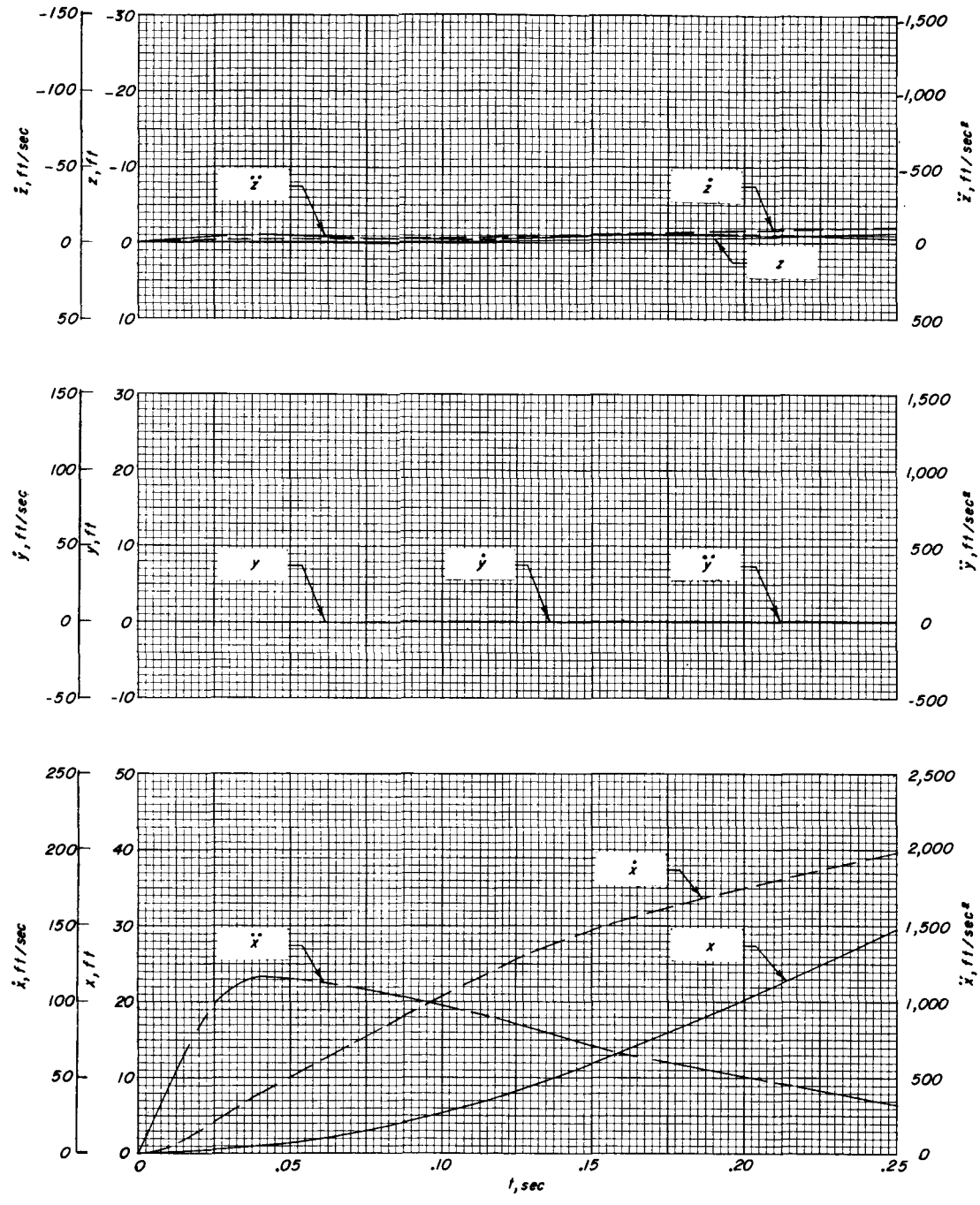


(a) Linear characteristics.

Figure 11.- Trajectory of round 4. Constant Mach number simulation; h ≈ 10,000 feet; M ≈ 0.27; $\alpha = 2.5^{\circ}$; $\beta = .0^{\circ}$; finite-length launcher.

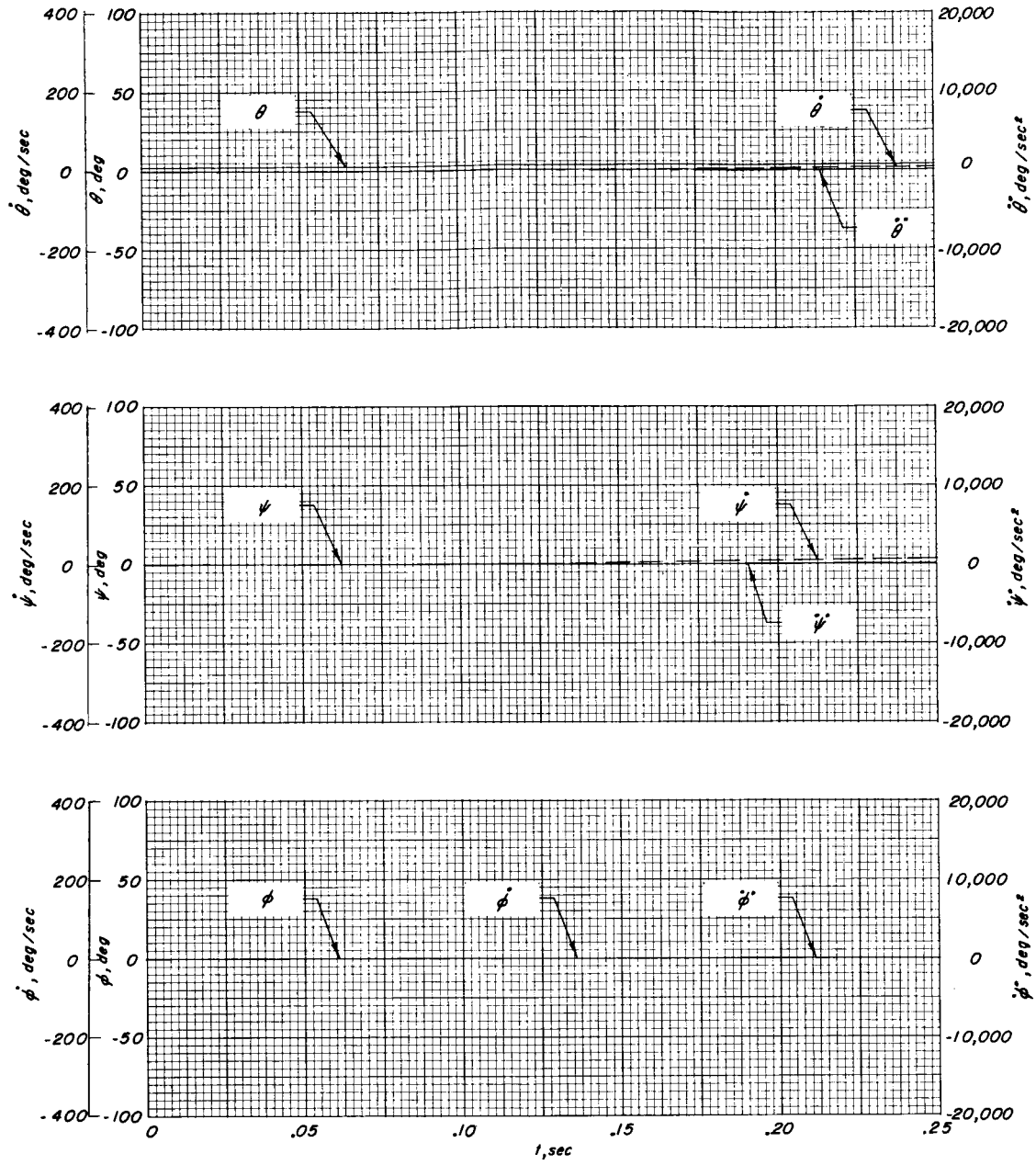


(b) Rotational characteristics.

Figure 11.- Concluded.

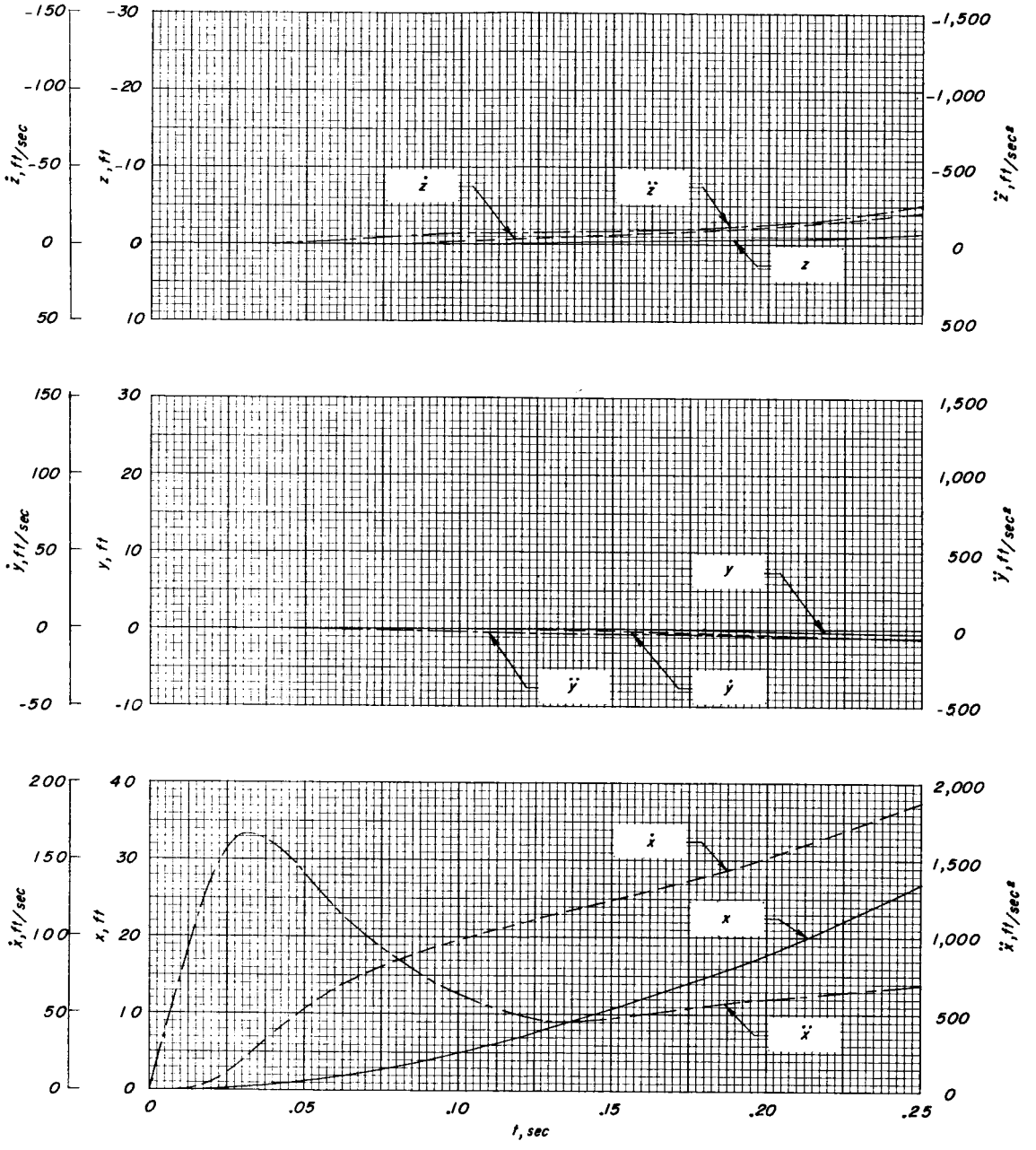


(a) Linear characteristics

Figure 12.- Trajectory of round 8. Constant Froude number simulation; h ≈ 10,000 feet; V corresponding to M = 0.80; $\alpha = 1.5^{\circ}$; $\beta = 0^{\circ}$; finite-length launcher.

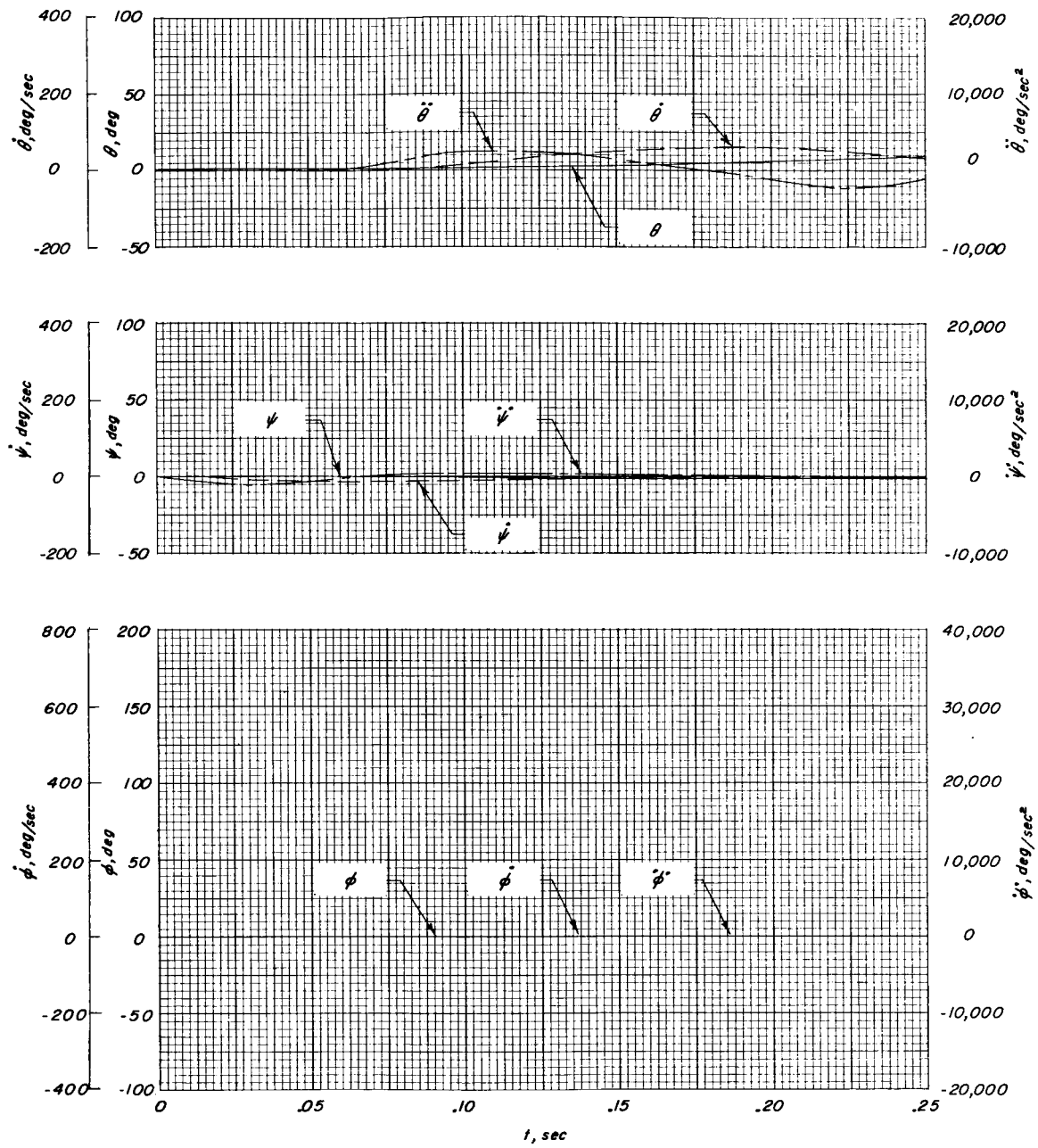


(b) Rotational characteristics.

Figure 12.- Concluded.

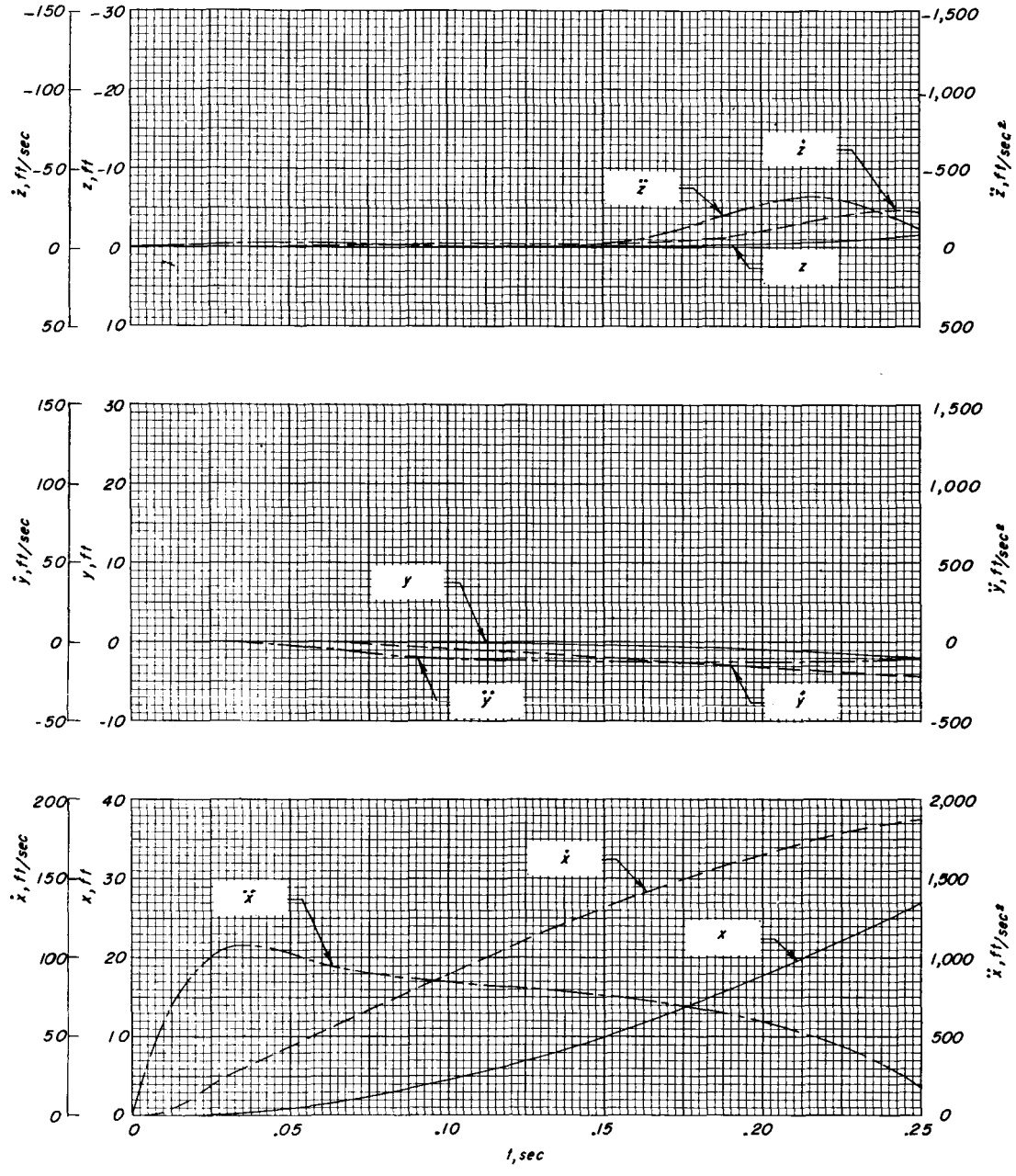


(a) Linear characteristics.

Figure 13.- Trajectory of round 9. Constant Froude number simulation; h ≈ 10,000 feet; V corresponding to M = 0.80; $\alpha = 1.5^{\circ}$; $\beta = 0^{\circ}$; zero-length launcher.

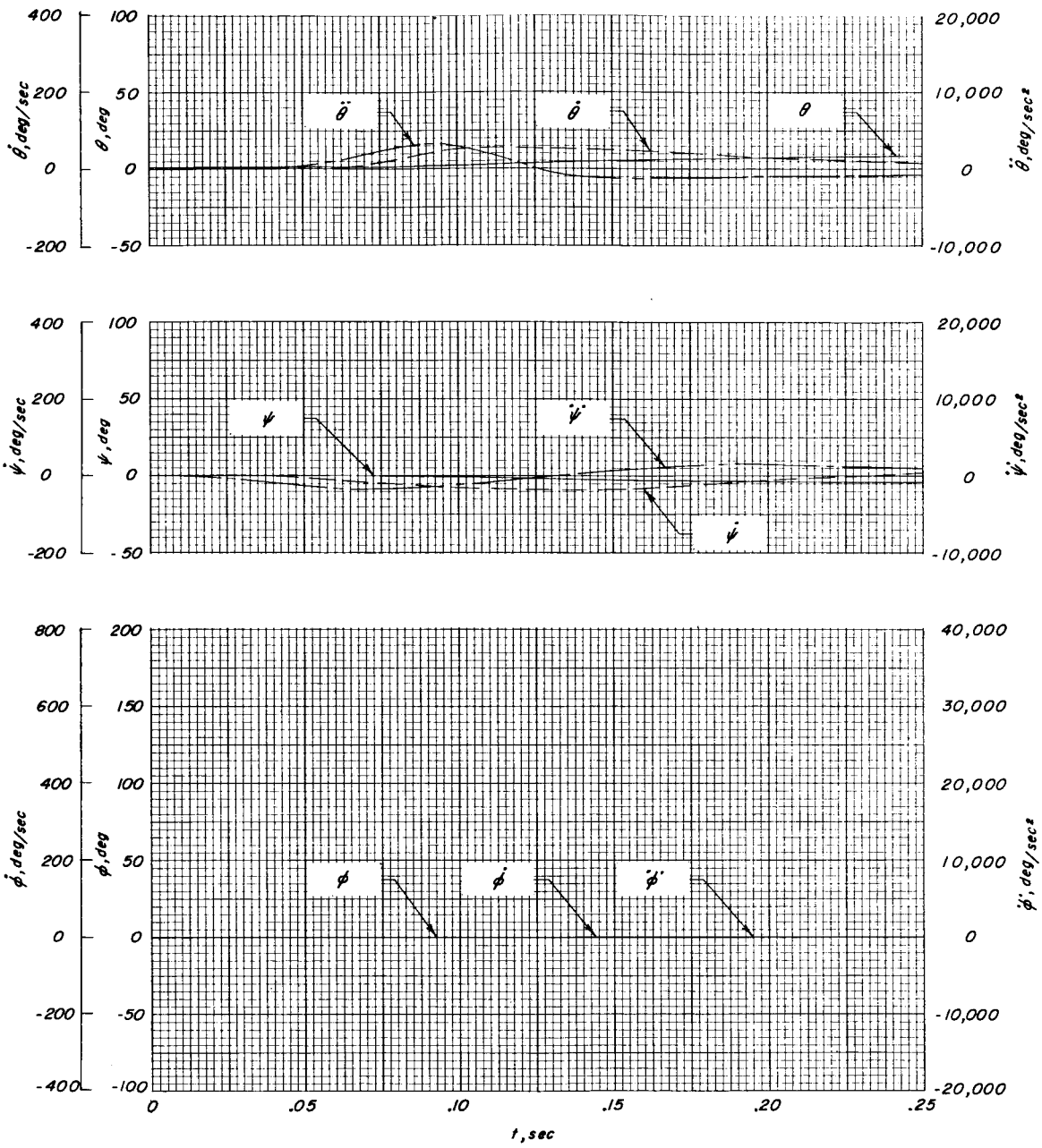


(b) Rotational characteristics.

Figure 13.- Concluded.

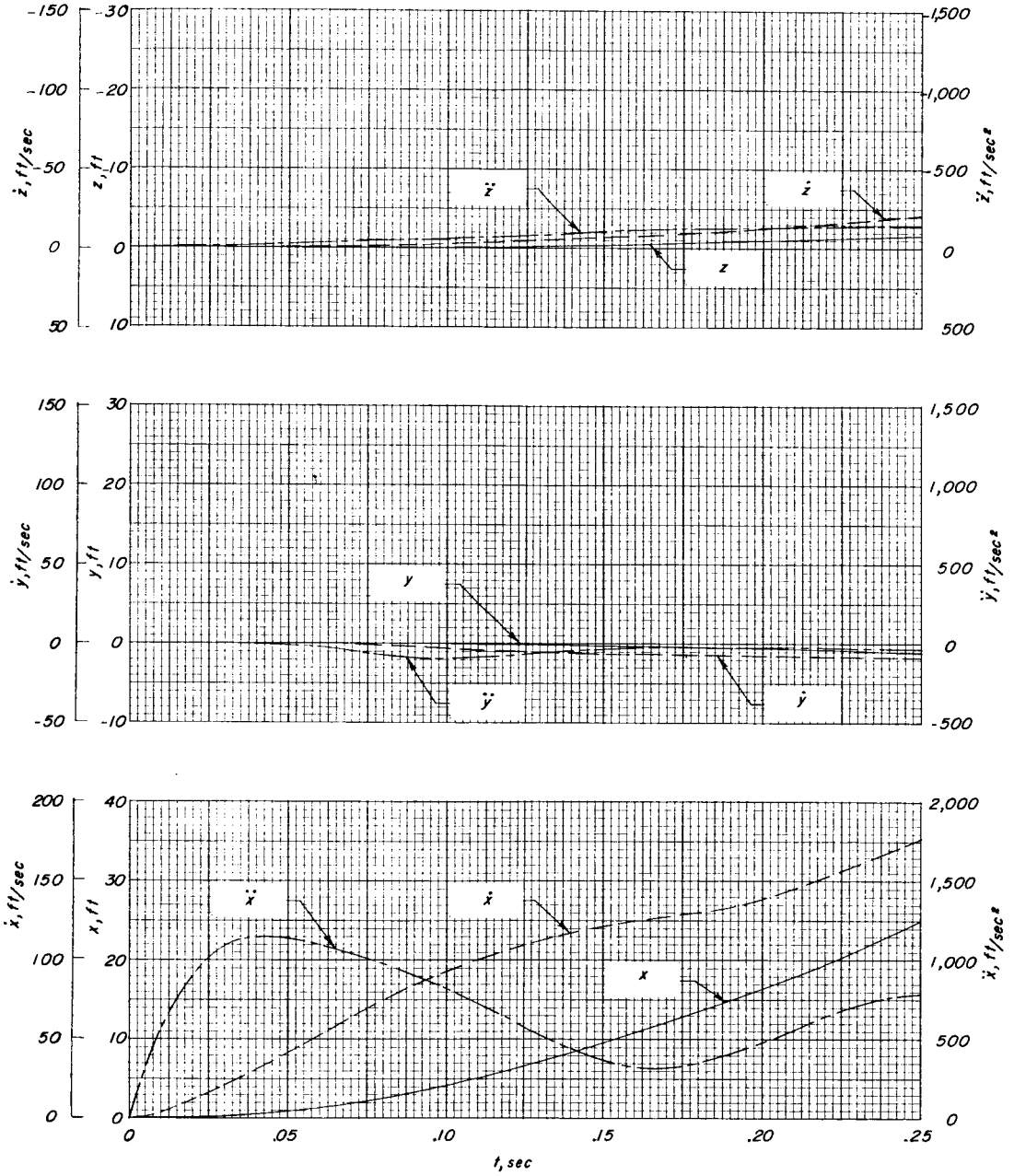


(a) Linear characteristics.

Figure 14.- Trajectory of round 10. Constant Froude number simulation; h ≈ 10,000 feet; V corresponding to M = 0.80; $\alpha = 2.6^{\circ}$; $\beta = 0^{\circ}$; zero-length launcher.

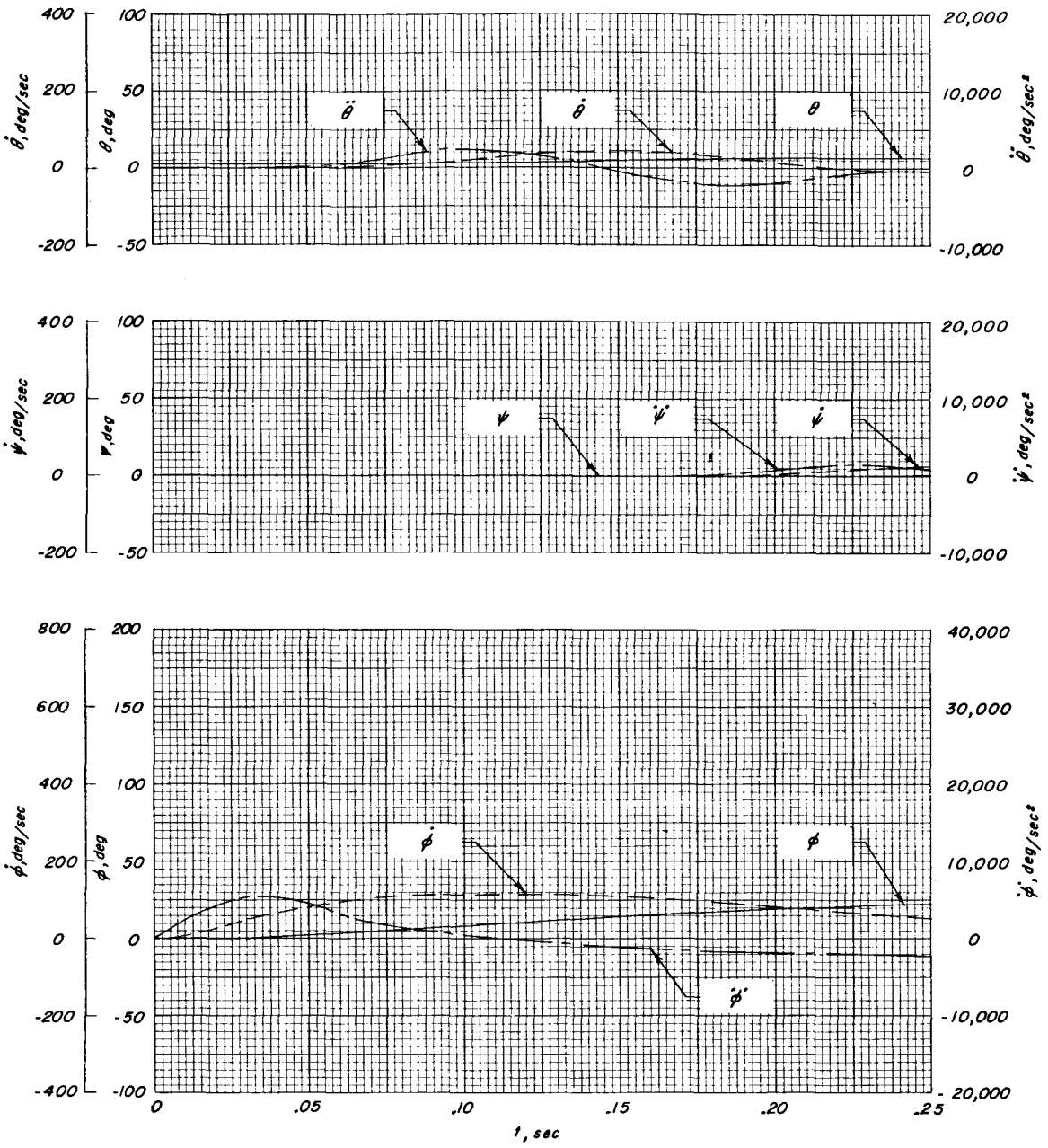


(b) Rotational characteristics.

Figure 14.- Concluded.

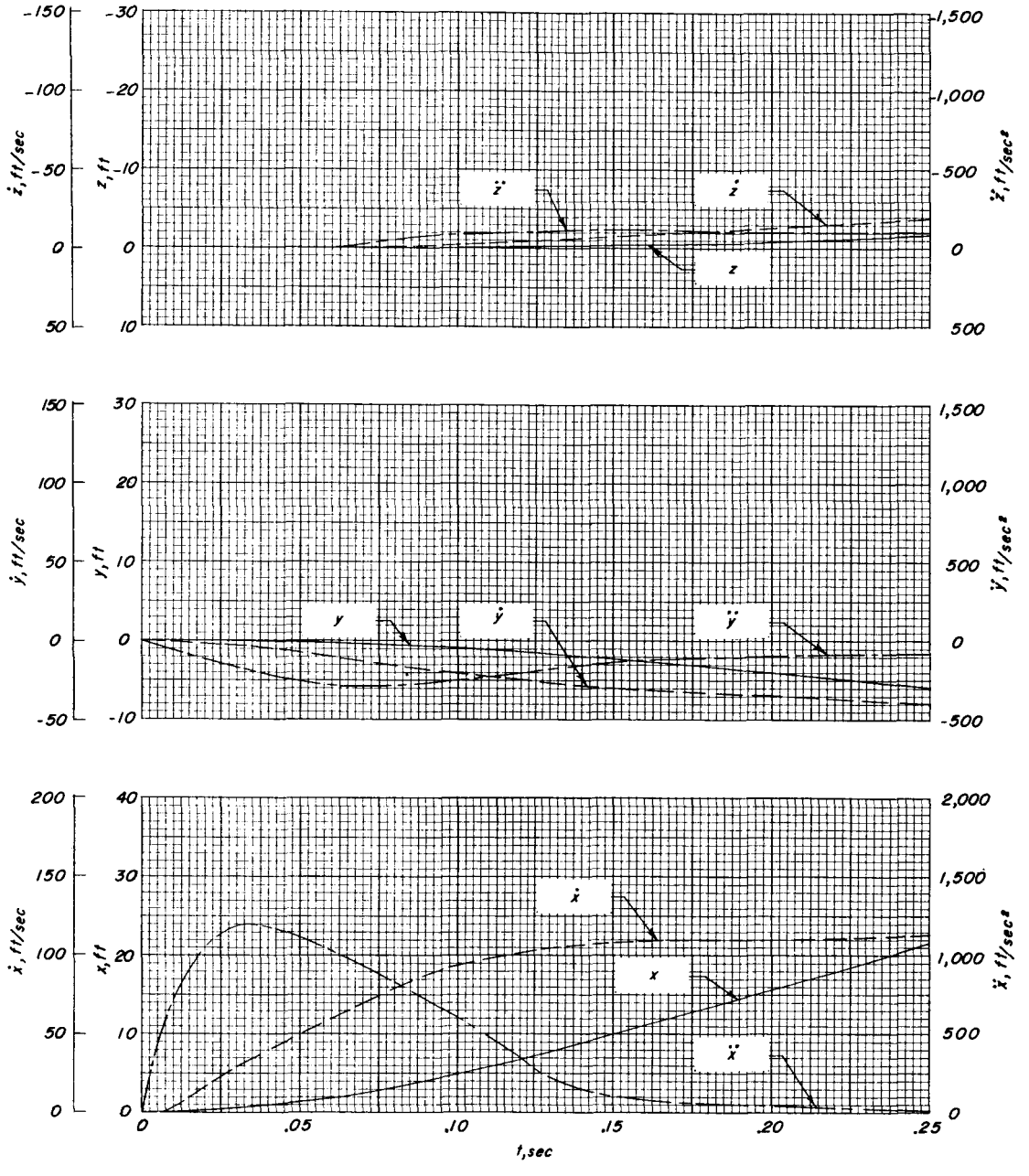


(a) Linear characteristics.

Figure 15.- Trajectory of round 11. Constant Froude number simulation; h ≈ 10,000 feet; V corresponding to M = 0.80; $\alpha = 1.5^{\circ}$; $\beta = 5^{\circ}$; zero-length launcher.

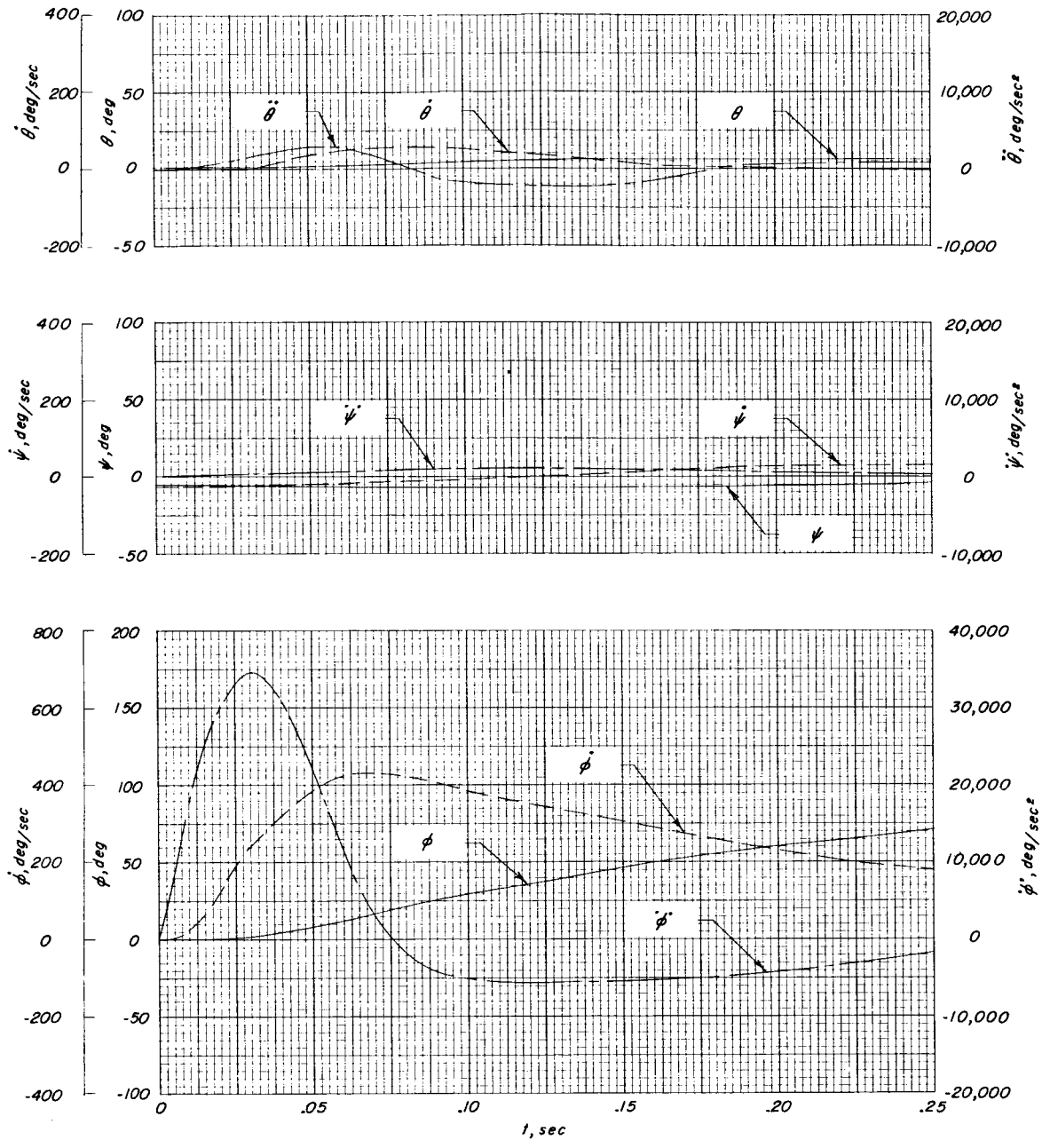


(b) Rotational characteristics.

Figure 15.- Concluded.

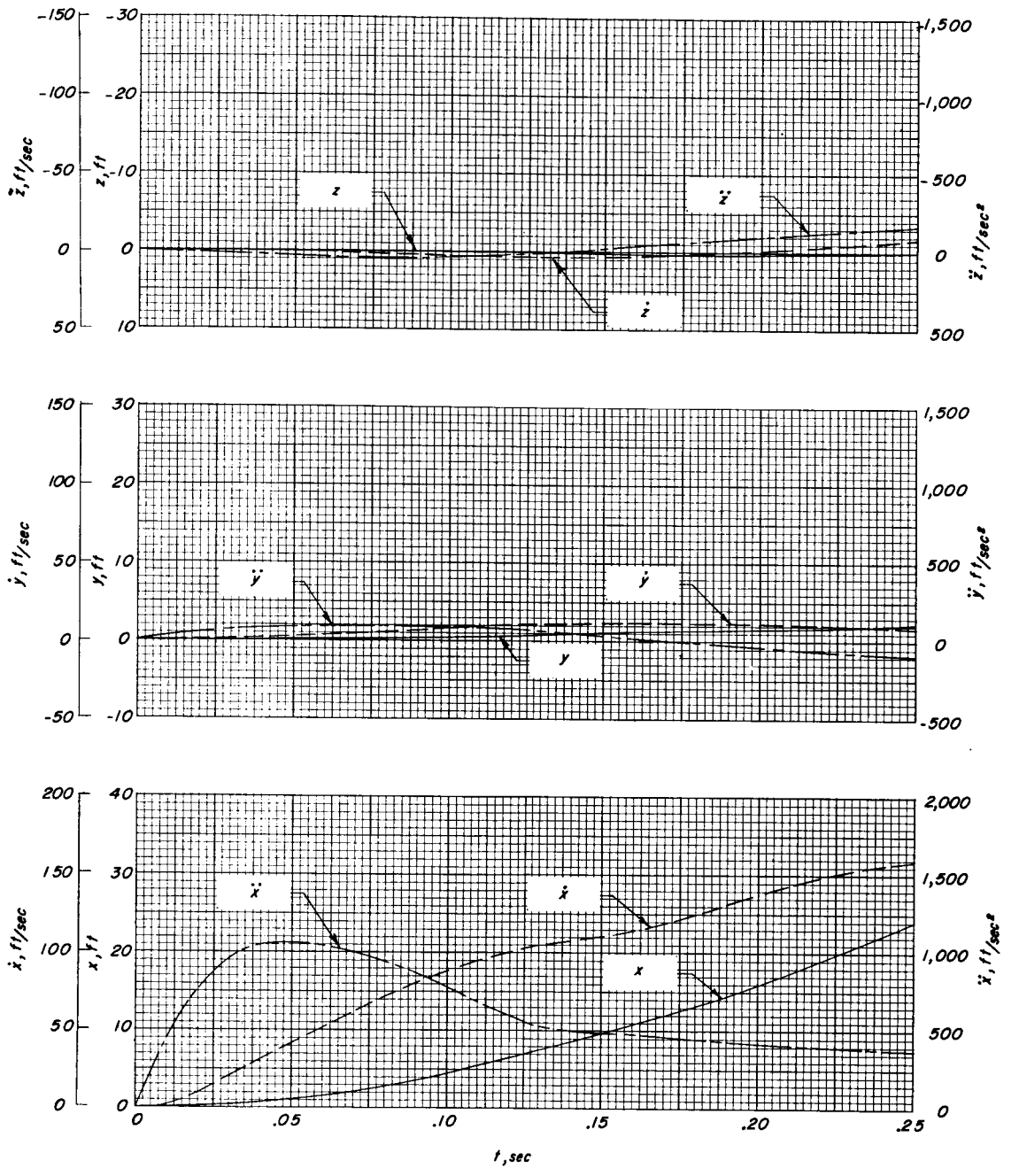


(a) Linear characteristics.

Figure 16.- Trajectory of round 12. Constant Froude number simulation; h ≈ 10,000 feet; V corresponding to M = 0.80; $\alpha = 1.5^\circ$; $\beta = -5^\circ$; zero-length launcher.

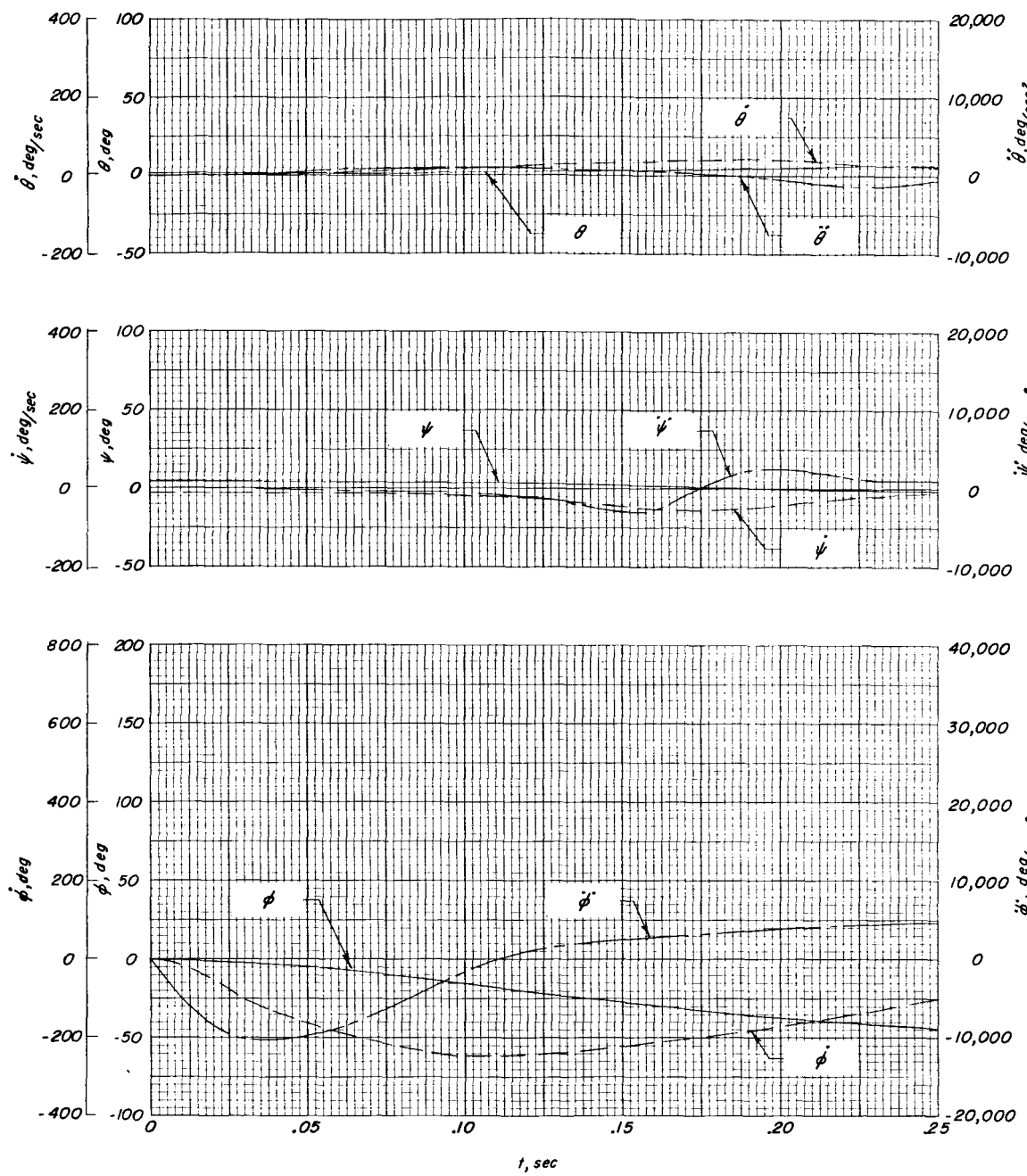


(b) Rotational characteristics.

Figure 16.- Concluded.

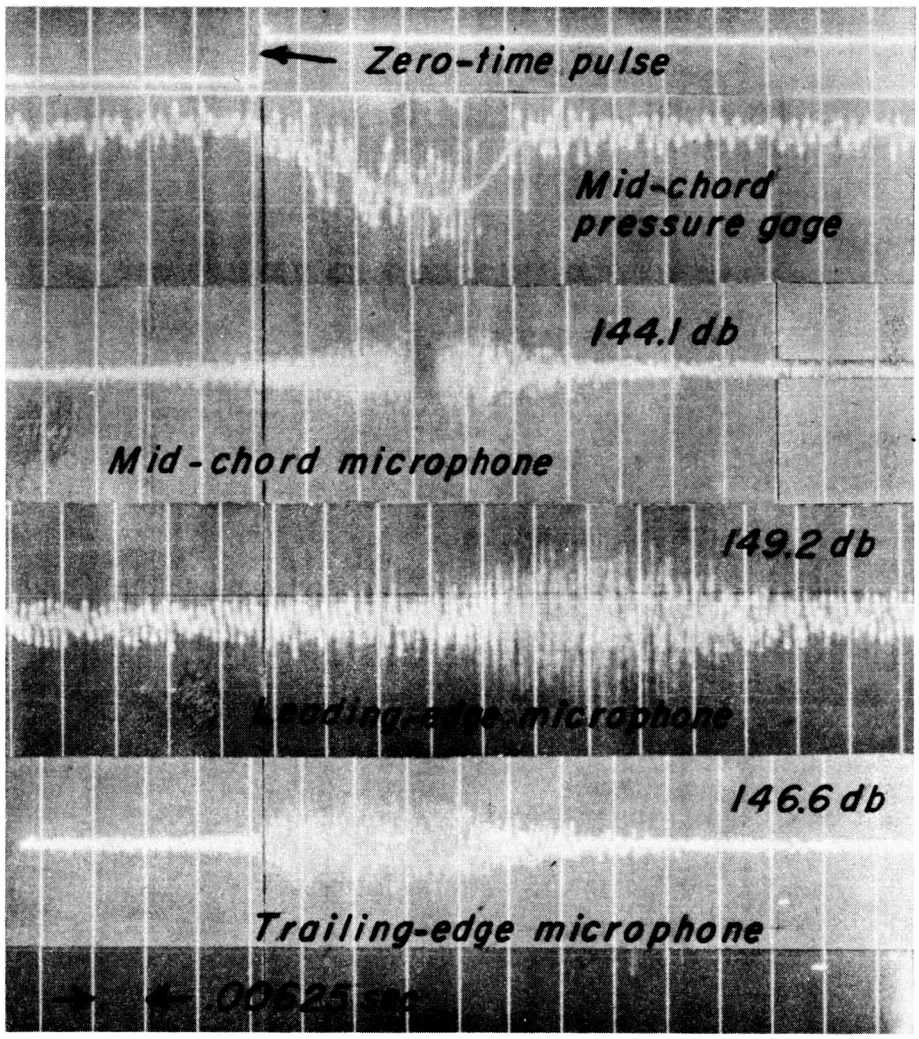


Figure 17.- Typical noise time histories of the missile traversing the wing lower surface.